Research Square

Preprints are preliminary reports that have not undergone peer review.
They should not be considered conclusive, used to inform clinical practice,
or referenced by the media as validated information.

Welding Metallurgy of Super Duplex Stainless Steel UNS S32750: A State-of-the-Art Review of GMAW Process Parameters, Microstructure–Property Relationships and Corrosion Performance

AMIT PANCHAL

abp@lecollege.ac.in

Lukhdhirji Engineering College https://orcid.org/0009-0001-8658-526X

Sagarkumar Indravadan Shah

Atmiya University

Jinesh Bipinbhai Shah

Atmiya University

Research Article

Keywords: Super duplex stainless steel, UNS S32750, gas metal arc welding, Gaussian process regression, pitting corrosion, heat input

Posted Date: November 12th, 2026

DOI: https://doi.org/10.21203/rs.3.rs-11499856/v1

License: This work is licensed under a Creative Commons Attribution 4.0 International License.
Read Full License

Welding Metallurgy of Super Duplex Stainless Steel UNS S32750: A State-of-the-Art Review of GMAW Process Parameters, Microstructure–Property Relationships and Corrosion Performance

Amit Bhalchandra Panchal[1,2,*] · Sagarkumar Indravadan Shah[3] · Jinesh Bipinbhai Shah[3]

[1]Atmiya University, Rajkot 360005, Gujarat, India (PhD Research Scholar)

[2]Production Engineering Department, L.E. College, Morbi 363642, Gujarat, India

[3]Mechanical Engineering Department, Atmiya University, Rajkot 360005, Gujarat, India

***Corresponding author:** Amit Bhalchandra Panchal, Production Engineering Department, L.E. College, Morbi 363642, Gujarat, India. E-mail: abp@lecollege.ac.in

E-mail addresses and ORCID iDs

Amit Bhalchandra Panchal: abp@lecollege.ac.in; ORCID https://orcid.org/0009-0001-8658-526X

Sagarkumar Indravadan Shah: sagarkumar.shah@atmiyauni.ac.in; ORCID https://orcid.org/0000-0001-8916-4922

Jinesh Bipinbhai Shah: jinesh.shah@atmiyauni.ac.in; ORCID https://orcid.org/0009-0001-9713-3349

Author contributions: Amit Bhalchandra Panchal: conceptualisation, methodology, literature search and data curation, formal analysis, visualisation, writing – original draft. Sagarkumar Indravadan Shah: conceptualisation, supervision, validation, writing – review and editing. Jinesh Bipinbhai Shah: methodology, validation, visualisation, writing – review and editing. All authors read and approved the final manuscript.

Article type: Review article

Abstract

Super duplex stainless steel UNS S32750 (SAF 2507) combines a pitting resistance equivalent number above 40 with high strength, but its properties depend on a ferrite–austenite balance that welding readily disturbs. Gas metal arc welding (GMAW) is productive, yet GMAW-specific evidence for this alloy remains limited. A structured narrative review (emphasis 2018–2026) synthesised GMAW-specific findings, drew comparative mechanisms from gas tungsten arc, submerged arc and beam welding, and examined Gaussian process regression (GPR) for parameter optimisation. Data were converted to net heat input and grouped by corrosion test method. Weld-metal ferrite is governed by cooling time through 1200–800 °C, nitrogen retention and ER2594 nickel over-alloying, whereas Cr_2N, secondary austenite and σ-phase arise mainly from multipass reheating and interpass temperature. Pulsed GMAW in Ar–He shielding with nitrogen backing met NORSOK M-601 requirements (30–70 % ferrite, ≥27 J at −46 °C) in 33 mm plate at 1.2–1.6 kJ mm^{-1} arc energy. Oxidising shielding additions introduce oxide inclusions that degrade pitting resistance. Electrochemical critical pitting temperatures fall from 58–92 °C in base metal to 45–71 °C in arc welds and rise linearly with austenite fraction. GPR-based Bayesian optimisation located welding optima within 12–25 experiments with quantified uncertainty, but has not yet been applied to super duplex GMAW. Fixed heat-input windows are incomplete because thickness, pass count and gas chemistry shift outcomes; above-guideline parameters are qualified only for heavy sections. Thermal-history-based qualification, nitrogen management, harmonised corrosion testing and constrained GPR optimisation of ferrite, toughness and pitting resistance are priorities.

Keywords: Super duplex stainless steel; UNS S32750; gas metal arc welding; Gaussian process regression; pitting corrosion; heat input

1 Introduction

1.1 Super duplex stainless steels and the place of UNS S32750

Duplex stainless steels (DSSs) are Fe–Cr–Ni–Mo–N alloys whose solution-annealed microstructure consists of approximately equal volume fractions of body-centred cubic δ-ferrite and face-centred cubic γ-austenite [1]. The two-phase structure provides yield strengths of roughly twice those of standard austenitic grades, good toughness, and a high resistance to chloride stress corrosion cracking, which has made these alloys standard materials in offshore oil and gas, desalination, pulp and paper, chemical processing and marine engineering [2]. Within the family, the super duplex grades are defined by a pitting resistance equivalent number (PREN = %Cr + 3.3%Mo + 16%N) of 40 or more [3,4]. UNS S32750 (EN 1.4410, commonly SAF 2507) is the most widely specified of them, with a nominal composition of 25Cr–7Ni–4Mo–0.27N [1,5]. Its combination of PREN around 42–43 and minimum yield strength of 550 MPa makes it a candidate for seawater-handling systems, subsea manifolds and umbilicals, heat exchangers and high-pressure process piping [2,3,6].

The same high alloy content that confers corrosion resistance also makes the alloy metallurgically sensitive. Chromium and molybdenum accelerate the precipitation of σ, χ and other intermetallic phases in the 600–1000 °C range, nitrogen supersaturation of ferrite promotes Cr_2N during rapid cooling, and α′ forms on prolonged exposure around 475 °C [7–10]. In UNS S32750, measurable σ-phase can begin to form within minutes at its nose temperature, considerably faster than in the 22Cr grades [4,11,12]. Any process that exposes the steel to repeated thermal cycles, of which fusion welding is the most common, therefore puts at risk both the phase balance on which the properties rest and the absence of precipitates on which the corrosion resistance depends [5,13,14].

1.2 Why gas metal arc welding

Gas tungsten arc welding (GTAW) remains the reference process for super duplex root passes and thin sections, because heat input and filler addition can be controlled independently [4,15,16]. Its deposition rate is, however, low, so pipelines, pressure vessels and thick-walled structures increasingly rely on gas metal arc welding (GMAW, also called MIG/MAG welding) for fill and cap passes, and in some cases for the full joint [6,17,18]. GMAW offers continuous wire feed, deposition rates several times those of GTAW, easy mechanisation and robotisation, and controlled-transfer variants such as pulsed spray and cold metal transfer (CMT) that decouple deposition from heat input [4,19,20]. The same arc physics underpins wire-arc additive manufacturing (WAAM), where super duplex

components are now being produced layer by layer with GMAW or CMT power sources [21–24].

GMAW also introduces variables that are less significant in GTAW: the shielding gas must sustain a stable consumable-electrode arc, which has historically led to small CO_2 or O_2 additions; the metal transfer mode affects droplet temperature and nitrogen loss; and dilution, travel speed and bead size are coupled to wire feed speed [25–28]. Consequently, recommendations derived from GTAW studies cannot simply be transferred to GMAW.

1.3 Previous reviews and objectives of this work

Several reviews have addressed welding of duplex alloys. Verma and Taiwade [13] critically reviewed processes and conditions for DSS and super DSS weldments; Pramanik et al. [14] and Patra et al. [29] discussed weldability and manufacturability; Mohammed et al. [30] focused on heat input; Maurya et al. [31] examined dissimilar joints with Ni alloys; Liu et al. [32] reviewed pitting and environmentally assisted cracking; and Zhang et al. [33] reviewed additive manufacturing of DSSs. Most recently, Li et al. [5] surveyed welding processes for UNS S32750, but their review is organised by process type and treats GMAW only briefly. To the authors' knowledge, no review has yet integrated GMAW process parameters, the resulting thermal and chemical history, microstructural evolution and the mechanical and corrosion performance of UNS S32750 into a single quantitative framework. Because GMAW-specific studies on UNS S32750 are still few (Section 4.2), the present review synthesises the available GMAW-specific findings and uses GTAW, shielded metal arc welding (SMAW), submerged arc welding (SAW) and high-energy-beam studies as comparative baselines for the mechanisms that are common to all fusion processes. Wherever data from a non-GMAW process are used, the process is stated explicitly, and heat-input values are normalised for thermal efficiency so that the comparison is not misleading (Section 2.3).

The objectives of this review are therefore to (i) summarise the physical metallurgy of UNS S32750 that is relevant to arc welding; (ii) critically assess how GMAW variables, namely arc energy, transfer mode, interpass temperature, shielding and backing gas, and filler metal, influence phase balance and secondary-phase formation; (iii) relate these microstructures to tensile, toughness, pitting, intergranular and hydrogen-assisted cracking behaviour; (iv) compile quantitative data from the literature into tabular and graphical summaries; and (v) identify gaps and priorities for research and for procedure qualification.

The overall process–structure–property–performance chain that structures the review is shown in Fig. 1.

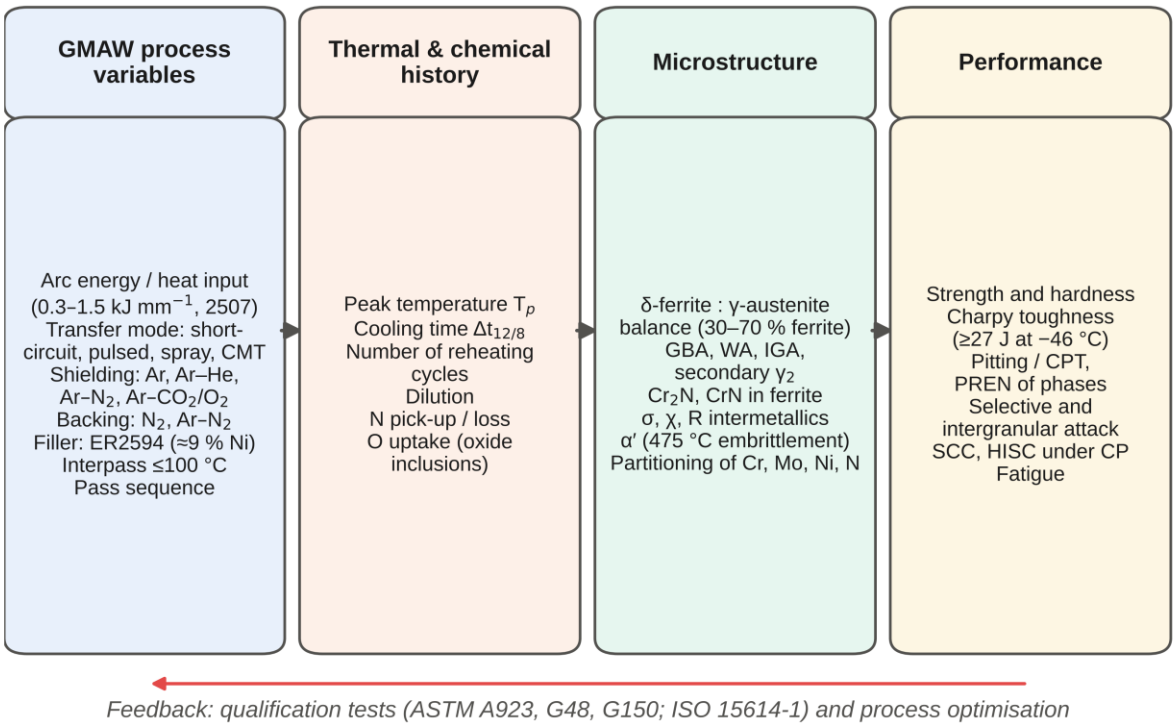


Fig. 1 Process–structure–property–performance chain for GMAW of UNS S32750: principal process variables, the thermal and chemical history they generate, the resulting microstructural features and the performance requirements, with feedback from qualification testing. Schematic compiled by the authors from [4,6,32,34]

2 Materials and methods

2.1 Review design and literature search

The review follows a structured narrative (semi-systematic) design. A core set of recent primary studies and reviews on welding of UNS S32750 and related duplex grades, together with the IMOA fabrication guidelines [4], formed the starting corpus. This corpus was extended by backward citation tracing of the reference lists of the core papers and by targeted keyword searches of web-based scholarly indexes and publisher platforms (Crossref metadata, Google Scholar, ScienceDirect, SpringerLink, Taylor & Francis Online, MDPI and Wiley Online Library). Search strings combined material terms ("super duplex", "UNS S32750", "SAF 2507", "2507", "ER2594", "25Cr duplex") with process terms ("gas metal arc", "GMAW", "MIG", "MAG", "pulsed", "cold metal transfer", "wire arc additive") and property terms ("ferrite", "austenite", "sigma", "chromium nitride", "secondary austenite", "pitting",

"critical pitting temperature", "toughness", "hydrogen"). A dedicated search on Gaussian process regression (GPR) and Bayesian optimisation applied to welding, additive manufacturing and corrosion, including the foundational statistical literature, supports Section 4.3. The full set of search strings is listed in Appendix A.

A generative artificial intelligence assistant based on a large language model (Claude, Anthropic) was used to support literature retrieval, drafting and language editing of the text, re-plotting of published numerical data and formatting of the manuscript. Every reference was checked against its publisher or DOI record, and the authors reviewed and edited all content and take full responsibility for it.

2.2 Inclusion criteria and quality appraisal

Peer-reviewed journal articles, standards and authoritative fabrication guidelines were included when they reported (a) welding or thermal simulation of UNS S32750 or a closely comparable 25Cr super duplex grade (UNS S32760, S32520) or (b) fundamental mechanisms of phase transformation, nitrogen behaviour or corrosion in duplex weld metals that apply directly to S32750. Studies on standard (2205) and lean duplex grades were retained where they provide the only GMAW-specific evidence for a mechanism, and this is indicated in the text. Publications from 2018 onwards were prioritised so that the review reflects the current state of knowledge, while older studies were kept where they remain the primary source for a mechanism. Each bibliographic record was checked against its DOI. Studies were appraised for completeness of process reporting (current, voltage, travel speed, thermal efficiency, interpass temperature, gas composition), the method used to quantify phases, and the corrosion test standard applied.

2.3 Data extraction and normalisation

For each primary study, the alloy, thickness, process and transfer mode, consumable, shielding and backing gas, arc energy or heat input, interpass temperature, phase fractions, secondary phases identified, and mechanical and corrosion results were extracted; the results are summarised in the tables of Section 3. Because authors report either arc energy ($E = U \cdot I/v$, i.e. $\eta = 1$) or heat input with their own efficiency factor, all heat-input values used in the compiled plots were converted to a common basis in two steps. First, each reported value was converted back to arc energy by dividing by the efficiency the authors stated (for example, $\eta = 0.65$ for SMAW [35] and $\eta = 0.8$ for robotic GMAW [18]); values reported with $\eta = 1$ [6,16] were used directly, and values for which no efficiency was stated [36] were treated as arc energy. Second, the net heat input was calculated as $Q = k \cdot E$ using the thermal efficiency

factors of EN 1011-1 [37]: k = 0.6 for GTAW, 0.8 for GMAW and SMAW, and 1.0 for SAW. Here U is the arc voltage, I the current and v the travel speed. The reported values, the efficiency used by each author, the factor applied and the resulting net heat input are listed for every data set in Table A1 (Appendix A), and all heat-input axes of the compiled data plots in Section 3 are net heat input. The guideline window of 0.3–1.5 kJ mm^{-1} for 2507 is defined as arc energy ($\eta = 1$) [4], so the process-window plot in Section 4.1 is drawn in arc energy for consistency with that guideline. Ferrite fractions measured by point counting, image analysis, magnetic induction (ferritescope) and electron backscatter diffraction were treated as comparable within about ±5 % only. Critical pitting temperatures (CPTs) were grouped by test method, namely chemical immersion in ferric chloride (ASTM G48 [38]) or electrochemical potentiostatic measurement (ASTM G150 [39]), because the two methods give systematically different values and are not directly comparable [6,16]; the two groups are kept separate in the corrosion data table and plots of Section 3.6.1. Compiled plots were generated only from values reported numerically in the cited studies.

2.4 Base and filler materials

The composition limits of UNS S32750 and the matching GMAW consumable are summarised in Table 1, together with representative certified analyses reported for a 33 mm plate and 1.2 mm ER2594 wire [6]. The filler is over-alloyed with nickel (about 9–10 % versus about 7 % in the plate) to promote austenite formation in the as-welded condition, while maintaining a weld-metal PREN comparable to that of the base metal [4,34]. The PREN values of UNS S32750 and of related grades and the consumable are compared in Fig. 2.

Table 1 Chemical composition (wt-%) of UNS S32750 base metal and the matching ER2594 GMAW consumable

Material	C	Si	Mn	Cr	Ni	Mo	N	Cu	W	PREN*
UNS S32750, specification limits [4]	≤0.030	≤0.80	≤1.20	24.0–26.0	6.0–8.0	3.0–5.0	0.24–0.32	≤0.50	–	40–43
UNS S32750, 33 mm plate (certified) [6]	0.015	0.34	0.74	24.97	6.89	3.80	0.275	0.20	0.046	42.0
ER2594 Ø1.2 mm GMAW wire (certified) [6]	0.015	0.40	0.61	25.23	9.22	4.04	0.260	0.09	0.04	42.8
ER2594 nominal (EN ISO 14343 G 25 9 4 N L) [4,34]	≤0.03	–	–	≈25	9–10	≈4	≈0.25	–	–	≈42

*PREN = %Cr + 3.3(%Mo + 0.5%W) + 16%N, calculated by the present authors from the listed compositions (W term included where reported). P and S (certified plate 0.021 and 0.001; wire 0.014 and 0.001) are omitted for brevity.

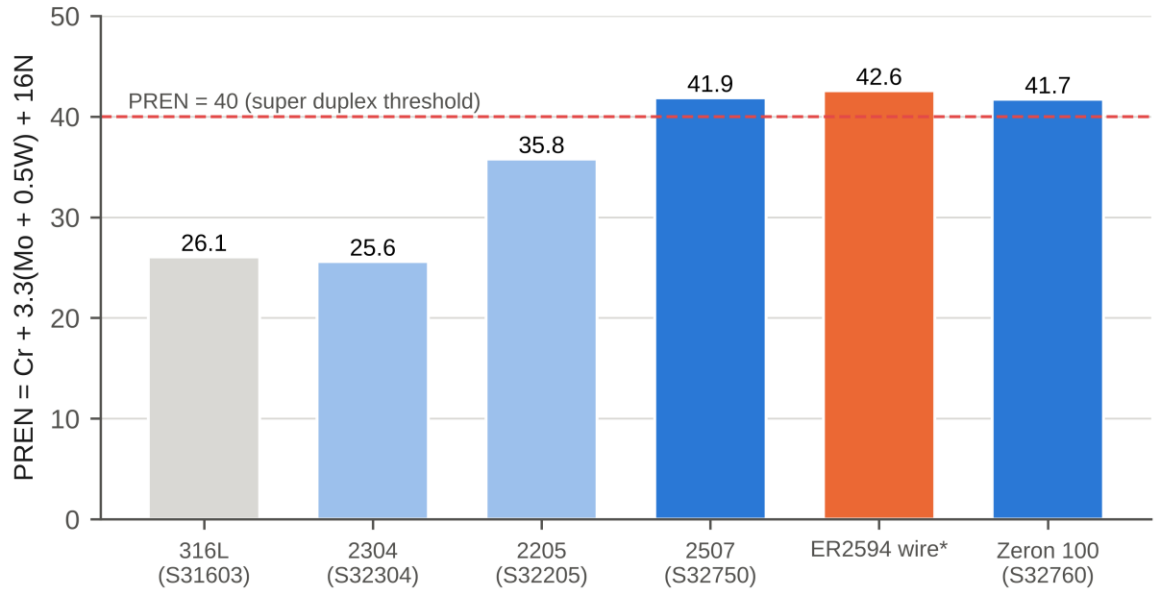


Fig. 2 Pitting resistance equivalent number (PREN = %Cr + 3.3(%Mo + 0.5%W) + 16%N) of UNS S32750 compared with austenitic 316L, lean (2304), standard (2205) and W-bearing super duplex (S32760) grades and with the ER2594 GMAW consumable. Nominal mid-range compositions [3,4]; ER2594 from the certified analysis of a 1.2 mm GMAW wire [6]. Calculated by the authors

2.5 Bibliometric overview of the reviewed literature

The distribution of the references cited in this review by publication period and theme is shown in Fig. 3. More than half of the cited works were published from 2018 onwards, which reflects both the growth of research on super duplex welding and the deliberate weighting towards recent evidence. Corrosion performance and microstructural evolution are the most heavily studied themes, whereas GMAW-specific studies on UNS S32750 remain comparatively few; much of the parameter-level evidence still comes from GTAW, SAW and standard duplex grades. The coverage of individual variables by the primary GMAW and arc-welding studies is mapped in Fig. 4, which shows that heat input and microstructure are almost always reported, but that shielding-gas chemistry, interpass temperature and hydrogen-related performance are reported much less often.

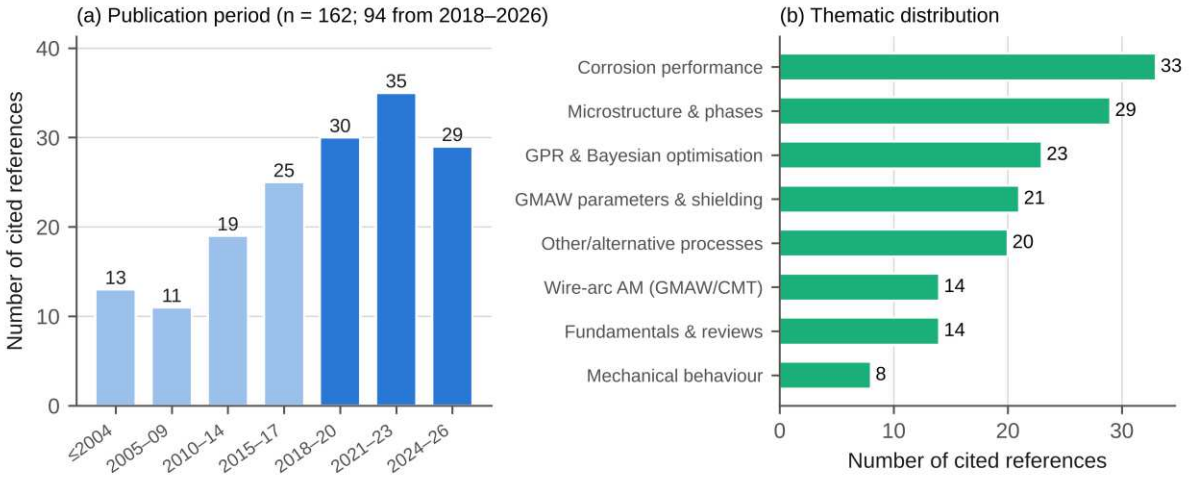


Fig. 3 Bibliometric overview of the references cited in this review: (a) distribution by publication period, with the 2018–2026 period highlighted; (b) distribution by principal theme. Compiled by the authors



Fig. 4 Coverage matrix of the principal primary studies reviewed (rows) against the process variables and properties they report (columns). Filled cells indicate that the variable or property was investigated. Totals per column are given below the matrix. Compiled by the authors from [6,16–18,25,27,28,35,36,40–51]

3 Data description

3.1 Physical metallurgy of UNS S32750 relevant to welding

3.1.1 Solidification and the ferrite-to-austenite transformation

UNS S32750 and its matching ER2594 weld metal solidify in the fully ferritic (F) mode [34,35]. On cooling, the weld metal therefore passes through a single-phase δ-ferrite field before austenite nucleates in the solid state below the ferrite solvus, at roughly 1350–1200 °C

depending on composition. Austenite first forms as allotriomorphic grain-boundary austenite (GBA), then grows as Widmanstätten side plates (WA) into the ferrite grains and, at lower temperatures or on reheating, as intragranular austenite (IGA) [35,45,52]. Because the transformation is diffusion-controlled, the final austenite fraction is governed by the time spent between about 1200 and 800 °C (often expressed as $\Delta t_{12/8}$) and by the driving force set by the austenite stabilisers nickel and nitrogen [34,53]. Fast cooling, as in autogenous laser, electron beam or low-energy GTAW welds, can leave fusion zones with 70–90 % ferrite [42,54,55], whereas slower cooling and higher nitrogen or nickel bring the balance close to 50:50 [43,56].

The austenite and ferrite that form are not of equal composition. Chromium, molybdenum and tungsten partition to ferrite, while nickel, nitrogen and to a lesser extent copper and manganese partition to austenite [1,45,57]. In the base metal, nitrogen raises the PREN of austenite until the two phases have similar resistance; in rapidly cooled weld metal, equilibrium partitioning is not achieved, so the PREN of each phase differs from that of the base metal and the weaker phase controls pitting [45,57,58]. Han et al. [45] found Ni and N enriched in the austenite and Cr and Mo in the ferrite of all zones of a UNS S32750 weldment, and selective corrosion of the lower-PREN ferrite in each zone.

3.1.2 Nitrogen

Nitrogen is the single most important alloying element in super duplex welding metallurgy. It is a strong austenite stabiliser, raises the temperature at which austenite forms on cooling, increases the strength of austenite and makes the largest contribution to its pitting resistance [1,4,59]. However, nitrogen solubility in liquid and δ-ferrite is limited, and nitrogen is lost from the weld pool and from the high-temperature heat-affected zone (HT-HAZ) during welding [60–62]. Hosseini et al. [60] documented nitrogen loss and its effects on the microstructure of multipass TIG welds of a super duplex grade, and physical and kinetic simulation confirmed nitrogen loss from the HT-HAZ at peak temperatures [61]. Varbai and Májlinger [62] combined physical and theoretical modelling to show that weld-metal nitrogen depends on both the shielding-gas composition and the heat input. The implication for GMAW is that nitrogen management through shielding and backing gas composition is as important as heat-input control.

3.1.3 Secondary phases

Table 2 summarises the secondary phases reported in welded UNS S32750 and their effects. Their formation windows are shown schematically in Fig. 5.

Table 2 Secondary phases reported in welded UNS S32750 and their effects

Phase	Structure / composition	Approximate formation range	Typical location in welds	Effect on properties	Key references
σ (sigma)	Tetragonal Fe–Cr–Mo intermetallic	≈600–1000 °C; fastest ≈850–900 °C	α/γ boundaries in reheated passes, LT-HAZ, root of thick multipass welds	Severe loss of toughness and pitting resistance at a few per cent	[6,7,10,63]
χ (chi)	Cubic, Mo-rich intermetallic	Lower part of σ range; often precedes σ	α/γ and α/α boundaries	Toughness and pitting loss; precursor to σ	[11,64]
Cr_2N / CrN	Hexagonal (cubic) chromium nitride	Rapid cooling from >1200 °C (quenched-in); isothermal ≈700–900 °C	HT-HAZ ferrite, root and cap passes, reheated weld metal	Cr-depleted zones; preferential pitting; nucleation of IGA	[8,45,52,65]
γ_2 (secondary austenite)	FCC; depleted in Cr, Mo, N	Reheating of ferrite-rich regions, ≈800–1000 °C and with σ	Reheated weld metal and HAZ in multipass joints	Lower local PREN; pitting site	[46,52,66,67]
α′ (alpha prime)	Cr-rich BCC (spinodal)	≈300–500 °C; "475 °C embrittlement"	Ferrite after long service or slow cooling of heavy sections	Hardening and loss of toughness	[4,9]
$M_{23}C_6$, R-phase	Carbide; Mo-rich intermetallic	Intermediate temperatures; minor in low-C grades	Occasionally in reheated passes	Local depletion; minor role in modern grades	[9,16]

Temperature ranges are approximate and composition-dependent; see the cited studies for kinetics.

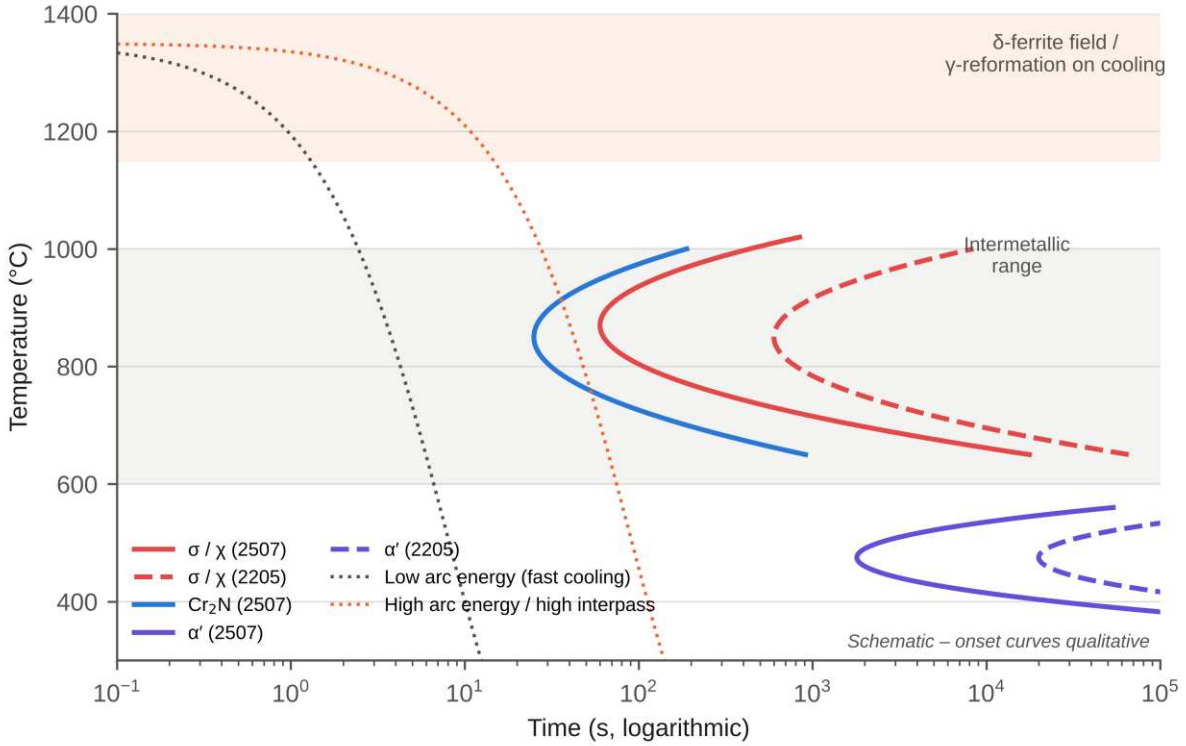


Fig. 5 Schematic time–temperature–precipitation diagram for UNS S32750 (solid lines) and 2205 (dashed lines), showing the onset of σ/χ, Cr_2N and α′ precipitation and representative weld cooling curves for low and high arc energy. The curves are qualitative and drawn after the kinetic data and guideline information in [4,7,8,11,12]

Chromium nitrides (mainly hexagonal Cr_2N, occasionally cubic CrN) precipitate in ferrite when cooling is too rapid for nitrogen to partition to austenite, because nitrogen solubility in ferrite falls sharply with temperature [8,52,65]. They are found predominantly in the HT-HAZ, in the root and cap passes and in the reheated weld metal, and are associated with Cr depletion and preferential pitting [6,45,68]. Pettersson et al. [8] characterised the precipitation of chromium nitrides in 2507 and its dependence on temperature and time. Holländer Pettersson et al. [65] demonstrated that Cr_2N particles can act as nucleation sites for intragranular austenite.

Secondary austenite (γ_2) forms when ferrite-rich weld metal or HAZ is reheated by subsequent passes, either as fine intragranular particles or as growth of existing austenite [52,66]. Because it forms at lower temperatures and partly by consuming Cr_2N, γ_2 is depleted in Cr, Mo and N relative to primary austenite, and therefore has a lower local PREN; it is a well-documented site of pitting in multipass super duplex welds [6,46,66]. The relationship between nitride dissolution and γ_2 formation was characterised in detail by Ramirez et al. [52].

Sigma (σ) is a tetragonal Fe–Cr–Mo intermetallic that nucleates at α/γ boundaries and grows into the ferrite between about 600 and 1000 °C, with fastest kinetics around 850–900

°C in super duplex grades [4,7,10]. Its growth produces a eutectoid-like reaction $\delta \rightarrow \sigma + \gamma_2$, which depletes the surrounding matrix of Cr and Mo [9,63]. Even a few per cent of σ severely reduces impact toughness and pitting resistance [7,10,69]. Chi (χ) is a cubic Mo-rich intermetallic that typically precedes σ at lower temperatures and is detected at α/γ and α/α boundaries [11,64]. The kinetics are strongly composition- and grain-size-dependent: Pardal et al. [63] found that grain size influences deleterious-phase precipitation in UNS S32750, and Calliari et al. [11] showed that continuous cooling of a 25Cr grade at slow rates produced σ and χ, whereas faster cooling suppressed them. Byun et al. [12] quantified the kinetics of Cr/Mo-rich precipitates in a 25Cr-6.9Ni-3.8Mo-0.3N steel.

At lower temperatures, α′ (a Cr-rich bcc phase) forms in ferrite by spinodal decomposition around 475 °C and causes hardening and loss of toughness, but it is mainly a concern for service and for slow-cooled heavy sections rather than for welding itself [4,9]. Carbides ($M_{23}C_6$) and R-phase are reported occasionally in reheated passes [9,16].

3.2 GMAW process fundamentals for super duplex stainless steels

3.2.1 Transfer modes and operating windows

GMAW of duplex stainless steels is performed with direct current, electrode positive. Three conventional transfer modes are available: short-circuiting transfer at low current and voltage, used mainly for thin sections and positional welding; globular transfer, which is generally avoided because of spatter and unstable arc behaviour; and spray transfer at higher current, which gives high deposition rates but also high heat input and is largely limited to the flat position [4,19]. Pulsed GMAW switches between a high peak current that detaches one droplet per pulse in spray mode and a low background current, so that spray-like transfer is obtained at a mean current, and thus heat input, in the short-circuit or globular range [4,6]. For super duplex steels, pulsed transfer is the most widely recommended mode because it combines controlled heat input, low spatter, good fusion and acceptable positional capability [4,6,17]. Typical GMAW parameter ranges from the IMOA guidelines, together with representative parameters used for super duplex and duplex welding in recent studies, are compared in Fig. 6.

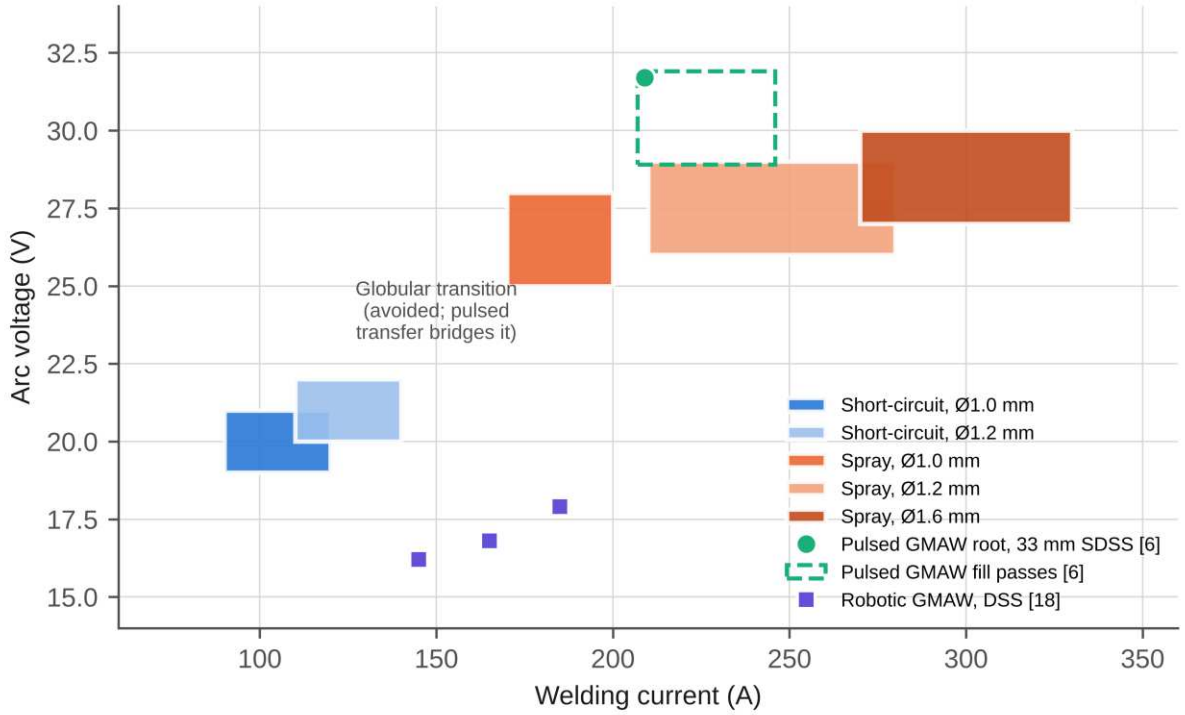


Fig. 6 GMAW operating windows (welding current and arc voltage) for duplex stainless steel wires of 1.0–1.6 mm diameter in short-circuit and spray transfer [4], compared with pulsed GMAW parameters used for 33 mm UNS S32750 plate [6] and robotic GMAW of 2205 [18]

Controlled short-circuit variants, of which CMT is the best known, retract the wire mechanically at each short circuit, reducing heat input and spatter further; these processes have been used mainly in WAAM of super duplex alloys [23,70,71]. Twin-wire GMAW increases deposition rate further; Hu and Xue [72] showed that the flow rate of an additional trailing shielding gas affected weld-seam properties in twin-wire GMAW of a duplex grade, which highlights the sensitivity of high-productivity variants to shielding. Hybrid TIG–MIG and laser–MIG processes combine a leading or trailing heat source with the GMAW arc to increase travel speed or penetration [73–75]. Weis et al. [73] found that pulsed and AC-pulsed MIG combined with TIG could join 2 mm 1.4462 duplex sheet at higher speed than conventional MIG, provided arc interaction (magnetic blow) was controlled by torch geometry and current modulation, and the joints passed ISO 15614-1 procedure tests.

3.2.2 Comparison with other fusion and solid-state processes

Table 3 compares GMAW with the other processes that have been applied to UNS S32750 and closely related super duplex grades. High-energy-density processes such as laser beam welding (LBW) and electron beam welding (EBW) produce narrow welds with high cooling rates and therefore excessive ferrite unless nitrogen, nickel or a post-weld heat treatment (PWHT) is applied [54,55,79,80]. Keyhole plasma arc welding gives deep

penetration in a single pass but also tends to ferritic fusion zones [77,78]. Activated-flux TIG increases single-pass penetration [83]. Solid-state processes such as friction stir welding (FSW) and linear friction welding (LFW) avoid solidification and preserve phase balance, but Cr_2N and σ can still form in the stir zone and the processes are limited in joint geometry and tool life [68,81,82,84]. Submerged arc welding (SAW) provides the highest deposition but is restricted to the flat position and thick sections [6]. GMAW occupies an intermediate position: it has higher productivity than GTAW and better positional capability than SAW, and its cooling rates lie between those of GTAW and LBW. This makes the selection of parameters, rather than of the process itself, the decisive factor.

Table 3 Qualitative comparison of welding processes applied to UNS S32750 and related super duplex grades

Process	Relative heat input / cooling rate	Productivity and positional use	Typical metallurgical concerns	Key references
GTAW (TIG)	Low–medium; fast cooling in autogenous passes	Low deposition; all positions; reference process for roots	Excess ferrite and Cr_2N in autogenous/root passes; γ_2 in multipass	[15,16,41,46]
GMAW (pulsed, spray, short-circuit)	Medium; adjustable through pulsing	High deposition; mechanisable; pulsed mode positional	N loss; oxide inclusions with CO_2/O_2; reheating of root in thick sections	[4,6,18,27]
CMT / controlled short-circuit	Low	Medium deposition; thin sections and WAAM	Ferrite-rich deposits; cumulative reheating in WAAM	[23,70,71]
Hybrid TIG–MIG / laser–MIG	Medium; high travel speed	High speed; mainly mechanised	Arc interaction; fast cooling of laser-dominated zones	[73–75]
SMAW / FCAW	Medium	Medium; site welding	Slag/oxygen pick-up; selective ferrite corrosion	[35,47,76]
SAW	High	Highest deposition; flat position, thick sections	σ and γ_2 if interpass temperature uncontrolled	[6]
Plasma arc (keyhole)	Medium–high energy density	Single-pass penetration up to medium thickness	Ferritic fusion zone without filler/N_2	[77,78]
Laser / electron beam	Very low; very fast cooling	High speed; precise fit-up needed	70–90 % ferrite, Cr_2N; needs N_2, Ni or PWHT	[43,54,79,80]
FSW / LFW (solid state)	No melting; severe deformation	Limited joint geometry; tool wear	Cr_2N and σ in stir zone; otherwise balanced phases	[68,81,82]

Qualitative ranking compiled from the cited studies; individual parameter values vary widely between studies.

3.3 Effect of GMAW parameters

The process conditions and principal findings of the main arc-welding studies discussed in this section are summarised in Table 4.

345 **Table 4** Summary of selected primary studies on arc welding of UNS S32750 and related duplex grades: conditions and principal findings

Ref.	Alloy / thickness	Process and consumable	Gas (shielding / backing)	Heat input (kJ mm⁻¹) / interpass	Principal microstructural findings	Principal property findings
[6]	S32750, 33 mm	Pulsed GMAW, ER2594 Ø1.2 mm, 18 passes; SAW	Ar–30 % He / N_2	AE (η = 1): GMAW 1.18–1.58 (net 0.94–1.26), IP 65–76 °C; SAW 1.2–1.5 and 2.0–2.3 (k = 1.0), IP ≤180 °C	WM ferrite 51–56 %, HAZ 61–65 %; σ only in GMAW root reheated by four passes	CVN −46 °C 72–253 J; CPT 45–60 °C (G48E); all joints met NORSOK M-601
[16]	S32750	Multipass GTAW, 105–180 A (8 to 3 passes)	Ar + 2 % N_2 / Ar + 2 % N_2	AE (η = 1) 0.78–1.47 (net 0.47–0.88); IP <100 °C	Ferrite 29.0→34.5 % with current; probable χ at 155–180 A	DOS 2.49→10.25 %; CPT (G150) 54→45 °C; optimum 0.78–0.99 kJ mm⁻¹ AE
[18]	2205	Robotic GMAW, 145–185 A	Ar–15 % CO_2	HI (η = 0.8) 0.44–0.62 (net same)	Pits at α/γ boundaries and HAZ in low-heat-input joint	Best corrosion behaviour at highest heat input (70 °C, 600 h)
[40]	2205	GMAW, parameters varied	n.r.	Varied	Bead geometry and cooling rate govern phase balance	–
[27]	2205	GMAW	Gas composition varied	n.r.	Shielding gas altered microstructure	Mechanical and corrosion properties changed with gas
[25]	Duplex and super duplex	GMAW and other processes	Several mixtures compared	n.r.	Gas affected weld geometry and weld-metal composition	Gas affected weld-metal properties
[36]	2205	GTAW (10/6/3 passes)	n.r.	Welding energy 0.5, 1.0, 3.5 (η not stated; net ≈0.3, 0.6, 2.1)	MZ ferrite 70→63→54 %; HT-HAZ 68→65→59 %; LT-HAZ 57→60→55 %	IGA in HAZ at 3.5 kJ mm⁻¹ (ASTM A262 A)
[41]	DSS and SDSS pipe	GTAW	Ar + 2 % or 5 % N_2 (shield and purge)	0.75–1.25; IP 120 and 160 °C	Grain coarsening and secondary phases at higher interpass temperature	Better strength and toughness at low heat input and 5 % N_2
[42]	S32750	Autogenous GTAW, preheat RT–300 °C	Ar, 15 L min⁻¹	n.r.	FZ austenite 15.8→16.5→25.8→42.4 %	Hardness 341→314 HV; fracture in base metal; corrosion approaches BM
[43]	S32750	Laser and hybrid GTAW–laser	Ar vs N_2 atmosphere	Arc current 20–40 A	FZ austenite 7.3–51.3 %	CPT 26–74 °C (G150); linear with austenite
[35]	S32750	SMAW, ER2594 vs ER2595	–	HI (η = 0.65) 0.80 / 0.74 (net ≈0.99 / 0.92)	Ferrite 68 % cap, 55 % root (ER2594); K–S orientation relation	ER2595 weld metal harder
[85]	S32750 / Nitronic 50	GTAW (dissimilar)	n.r.	0.61–1.01	Weld-zone ferrite decreased with heat input	Properties depend on heat input
[44]	S32750	GTAW, several filler rods	n.r.	n.r.	Filler choice changed phase balance	Strength and pitting resistance depend on filler
[17]	Super duplex, 12 mm	Multipass arc process combinations	n.r.	n.r.	Process combination changed microstructure	Mechanical and corrosion behaviour differed
[45]	S32750	TIG	Ar	n.r.	Three austenite morphologies; Cr_2N in HT-HAZ; Ni, N in γ and Cr, Mo in α	Selective corrosion of ferrite; similar passive films in all zones
[46,86]	Super duplex	Multipass TIG / repeated thermal cycles	n.r.	n.r.	γ_2 and nitrides in reheated HAZ and weld metal	Reduced corrosion resistance of reheated root
[47,87]	Super duplex, up to 20 mm	Bead-by-bead SMAW; multipass	n.r.	n.r.	Most-reheated beads contain most γ_2 and occasional σ	Reheating history governs local properties
[28]	Duplex (WAAM)	GMAW-based deposition	Ar vs Ar–2 % O_2 (20 L min⁻¹)	n.r.	≈0.1 % O with O_2; oxide inclusions, more γ_2 and IGA; γ > α in both walls	Passive film 87.3 vs 14.0 nm; i(corr) 13 vs 49 μA cm⁻²; E(corr) −30 vs −69 mV
[23,51]	ER2594 wall	CMT	n.r.	n.r.	Microstructural evolution under	Mechanical and corrosion behaviour

Ref.	Alloy / thickness	Process and consumable	Gas (shielding / backing)	Heat input (kJ mm^{-1}) / interpass	Principal microstructural findings	Principal property findings
	(WAAM)				thermal ageing and solution treatment	characterised

n.r. = not reported in the information extracted for this review; AE = arc energy; HI = heat input as reported; net = net heat input with EN 1011-1 factors (Table A1); IP = interpass temperature; WM = weld metal; MZ/FZ = molten/fusion zone; DOS = degree of sensitisation; CVN = Charpy V-notch energy. Heat input values as reported by the authors (thermal efficiency conventions differ).

3.3.1 Heat input, arc energy and cooling rate

Heat input controls both the cooling time through the austenite-formation range and the time spent in the intermetallic range, so its effect on super duplex welds is two-sided [4,13,30]. Too low a heat input produces fast cooling, high ferrite and nitride precipitation; too high a heat input, especially combined with high interpass temperature and thin sections, prolongs exposure at 600–1000 °C and promotes σ, χ and γ_2 [4,6,16]. The IMOA guidelines recommend 0.3–1.5 kJ mm^{-1} for 2507, compared with 0.5–2.5 kJ mm^{-1} for 2205 [4].

Compiled data on weld-metal ferrite versus net heat input are shown in Fig. 7a; all values were converted with the EN 1011-1 factors described in Section 2.3 (Table A1). For 2205 joints welded with GTAW, Pereira et al. [36] reported a fall in molten-zone ferrite from about 70 % at a welding energy of 0.5 kJ mm^{-1} to 63 % at 1.0 kJ mm^{-1} and 54 % at 3.5 kJ mm^{-1} (net heat input about 0.3, 0.6 and 2.1 kJ mm^{-1}). For UNS S32750 multipass GTAW of 8.2 mm pipe with Ar + 2 % N_2 shielding, Ketabi et al. [16] reported arc energies of 0.78–1.47 kJ mm^{-1} (η = 1; net heat input about 0.47–0.88 kJ mm^{-1}) and austenite-rich weld metal in which the ferrite fraction rose from 29.0 to 34.5 % as the current was increased from 105 to 180 A (Fig. 8a). In the interpretation adopted in this review, this opposite trend reflects the number of reheating cycles rather than the single-pass cooling rate: the joint welded at 105 A required eight passes, whereas that welded at 180 A required three, so the low-current weld metal was reheated more often and contained more secondary and reformed austenite. This distinction is annotated in Fig. 7a. The comparison is not entirely clean, because Pereira et al. also used fewer passes at higher energy (10, 6 and 3 passes) [36]; however, their welds started from a ferrite-rich condition (54–70 %) without nitrogen in the shielding gas reported, whereas the nitrogen-shielded welds of Ketabi et al. were already austenite-rich, so the additional reheating cycles had a proportionally larger effect. Pulsed GMAW of 33 mm UNS S32750 plate at an arc energy of 1.18–1.58 kJ mm^{-1} (net about 0.94–1.26 kJ mm^{-1}) gave a mean weld-metal ferrite of 56 %, and SAW at 1.2–2.3 kJ mm^{-1} (k = 1.0) gave 51–53 % [6]. For SMAW of UNS S32750 with ER2594 electrodes, Dandekar et al. [35] reported a heat input of 0.80 kJ mm^{-1} with η = 0.65, which corresponds to a net heat input of about 0.99 kJ mm^{-1} on the EN 1011-1 basis, and 68 % ferrite in the cap and 55 % in the root. Together, these results indicate that, for the industrially relevant net heat-input range of about 0.5–1.3 kJ mm^{-1}, heat input alone does not determine phase balance; the number of passes, section thickness, shielding gas and filler nickel content shift the result by a similar amount.

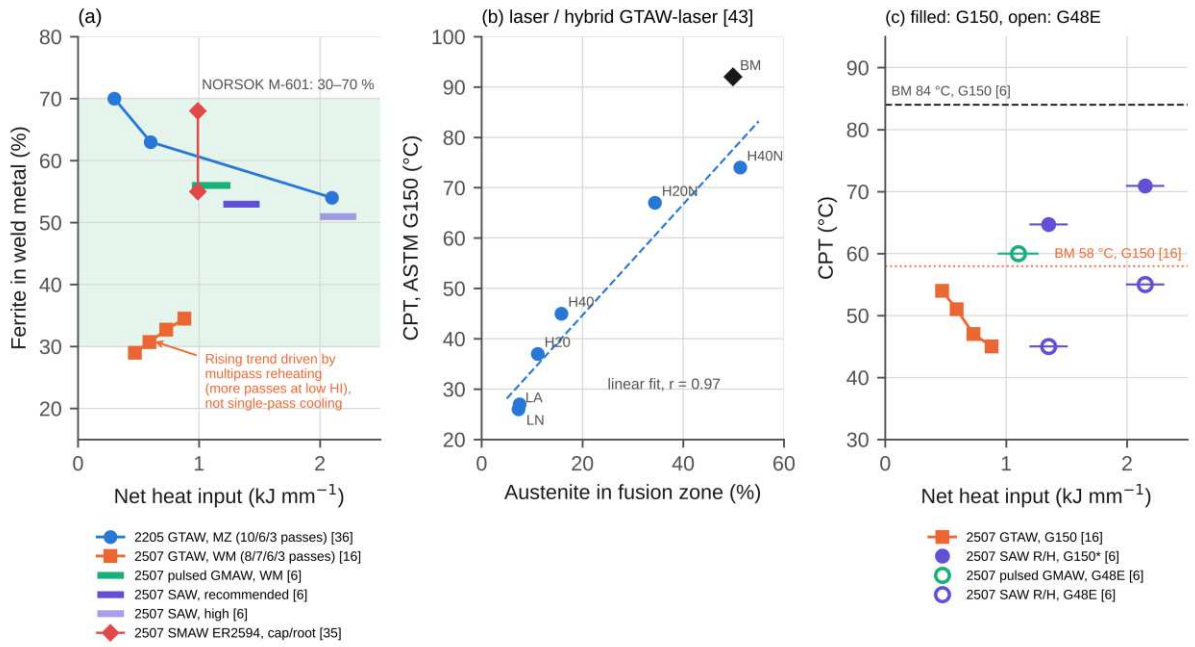


Fig. 7 Compiled literature data: (a) weld-metal ferrite as a function of net heat input for GTAW, pulsed GMAW, SAW and SMAW joints [6,16,35,36]; the rising trend of Ketabi et al. is annotated because, in the interpretation adopted here, it is driven by the larger number of reheating passes at low current (8 passes at 105 A versus 3 at 180 A) rather than by single-pass cooling rate; (b) critical pitting temperature (ASTM G150) versus fusion-zone austenite for laser (LA, LN) and hybrid GTAW–laser welds made in argon (H20, H40) or nitrogen (H20N, H40N) and the base metal (BM) [43]; (c) critical pitting temperature versus net heat input, with electrochemical ASTM G150 values as filled symbols and immersion ASTM G48E values as open symbols [6,16]. All heat inputs were converted to net heat input with the EN 1011-1 factors k = 0.6 (GTAW), 0.8 (GMAW, SMAW) and 1.0 (SAW) after removing the efficiency used by each author (Table A1) [37]. Horizontal bars span the reported range. Values replotted by the authors from the numerical data reported in the cited studies

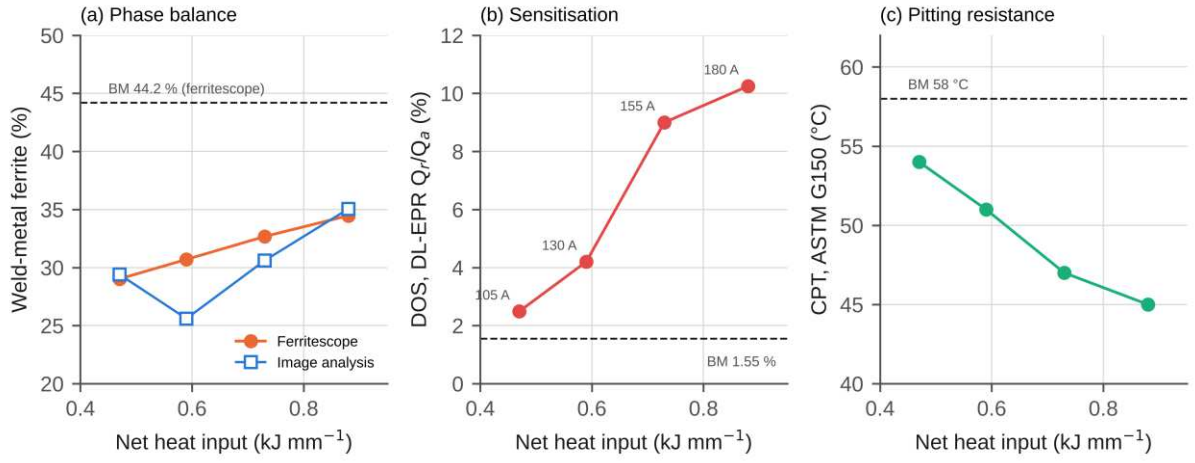


Fig. 8 Effect of heat input on multipass GTAW joints of 8.2 mm UNS S32750 pipe welded with Ar + 2 % N_2 at 105, 130, 155 and 180 A (8, 7, 6 and 3 passes): (a) weld-metal ferrite measured by ferritescope and image analysis; (b) degree of sensitisation from DL-EPR tests (charge ratio Qr/Qa); (c) critical pitting temperature (ASTM G150). Dashed lines show base-

metal values. Heat input converted to net heat input (k = 0.6). Replotted by the authors from the data of Ketabi et al. [16]

For GMAW of duplex grades specifically, Miranda-Pérez et al. [18] produced robotic GMAW joints at 0.44–0.62 kJ mm^{-1} with Ar–15 % CO_2 shielding and exposed them in an accelerated corrosion reactor at 70 °C for 600 h. The joint with the highest heat input showed the best corrosion behaviour, and the low-heat-input joint showed the most damage, with pits at the α/γ boundaries and in the HAZ. Chacón-Fernández et al. [40,88] showed for 2205 and S32001 joints that GMAW parameters controlling bead geometry and cooling rate govern the phase balance. For UNS S32750 joints made by other arc processes, low heat input has been associated with higher strength and toughness in GTAW [15,41], while excessive heat input was associated with intermetallic precipitation, a lower CPT and a higher degree of sensitisation [16,89]. In dissimilar S32750/Nitronic 50 GTAW joints, Maurya et al. [85] found that increasing heat input from 0.61 to 1.01 kJ mm^{-1} reduced ferrite in the weld zone. Kumar et al. [90] similarly reported an influence of heat input on phase balance and mechanical performance of GTAW super duplex welds.

3.3.2 Interpass temperature and multipass reheating

In multipass welding, each deposited bead is reheated by subsequent passes, and a given volume can pass through the 600–1000 °C range several times (Fig. 9). The IMOA guidelines limit interpass temperature to 100 °C for super duplex grades and 150 °C for standard and lean grades [4]. Paulraj and Garg [41] found that raising the interpass temperature of S32750 GTAW pipe welds from 120 to 160 °C reduced strength and toughness, which they attributed to grain coarsening and secondary-phase precipitation.

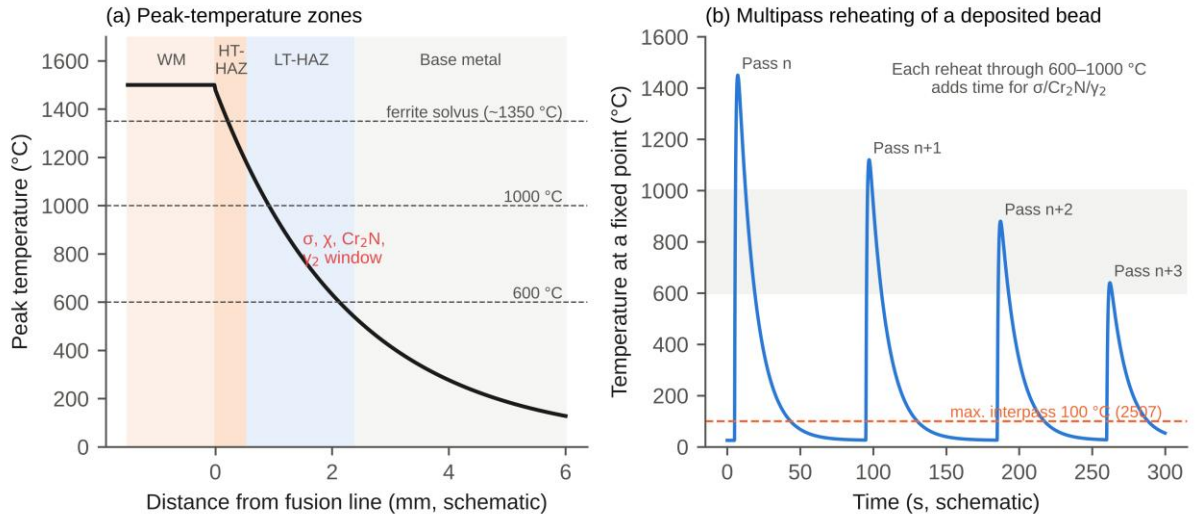


Fig. 9 Thermal history of a multipass GMAW joint (schematic): (a) peak-temperature zones of the weld and heat-affected zone and their characteristic microstructures; (b) successive

reheating of a deposited bead by subsequent passes, illustrating the cumulative time spent in the 600–1000 °C intermetallic range. Drawn by the authors after [4,6,47,91]

The most detailed bead-by-bead studies have been carried out at University West. Hosseini et al. [46,86] showed that multiple thermal cycles in TIG-welded super duplex steel produced γ_2 and nitrides in the HAZ and weld metal and reduced the corrosion resistance of the reheated root. In a 20 mm multipass joint and in a bead-by-bead SMAW study, the most-reheated beads contained the most γ_2 and occasional σ [47,87]. Valiente Bermejo et al. [6] extended this work to 33 mm UNS S32750 welded with pulsed GMAW (18 passes) and SAW. In the GMAW joint, σ was found only in a few locations of the root pass, which had been reheated by four subsequent passes, and γ_2 was concentrated in the passes reheated most often. The zone-resolved ferrite contents of the three 33 mm weldments are compared in Fig. 10a: all zones lay within 49–65 %, the HAZ was the most ferritic zone in each joint, and the GMAW weld metal was slightly more ferritic than the SAW weld metal, consistent with its lower net heat input per pass. Importantly, SAW at 2.0–2.3 kJ mm^{-1} with an interpass temperature of up to 180 °C, well above the recommended limits, still met the microstructural, toughness and corrosion requirements of NORSOK M-601 while halving the number of passes (17 to 8) and reducing the arc time for a 0.5 m weldment from 55.5 min for GMAW and 26.7 min for SAW at recommended settings to 18.9 min (Fig. 10b). The authors concluded that current recommendations for thick sections are conservative and should be revised. This finding illustrates that, for thick sections, fewer reheating cycles can outweigh a higher peak heat input. It must not, however, be generalised: the 33 mm plate provided three-dimensional heat flow and fast cooling between passes, and the same arc energy and interpass temperature applied to thinner sections or to joints with fewer heat sinks would lengthen the time in the 600–1000 °C range and could promote σ embrittlement. This is which is consistent with the pass-count effect observed by Ketabi et al. [16].

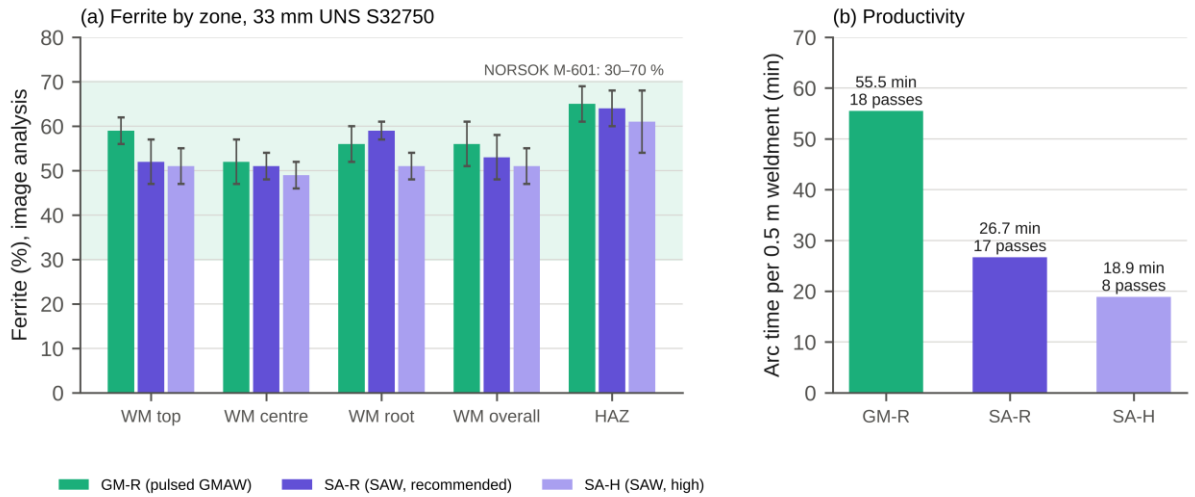


Fig. 10 Experimental data for 33 mm UNS S32750 plate welded by pulsed GMAW (GM-R) and by SAW at recommended (SA-R) and higher-than-recommended (SA-H) arc energy and interpass temperature: (a) ferrite content (image analysis, mean ± standard deviation) in the top, centre and root of the weld metal, the overall weld metal and the HAZ, with the NORSOK M-601 acceptance band; (b) arc time to complete a 0.5 m weldment and number of passes. Replotted by the authors from the data of Valiente Bermejo et al. [6]

Preheating is generally not required for duplex steels, but it has been explored as a means of slowing cooling in thin sections. Da Cruz Junior et al. [42] increased the fusion-zone austenite of autogenous bead-on-plate GTAW UNS S32750 welds from 15.8 % at room temperature to 16.5, 25.8 and 42.4 % with substrate preheats of 100, 200 and 300 °C, respectively, with a corresponding drop in hardness from 341 to 342, 327 and 314 HV and a corrosion response approaching that of the base metal (Fig. 11b and (c)). A preheat of at least 200 °C was needed to exceed 25 % austenite, and even 300 °C did not restore the 50 % austenite of the base metal; all tensile specimens nevertheless fractured in the base metal. Comparable effects of preheating on phase balance have been reported for laser-welded lean duplex steel [92]. Numerical approaches are increasingly used to predict these thermal histories; for example, Prunbauer et al. [93] developed a material model for SAF 2507 under welding conditions.

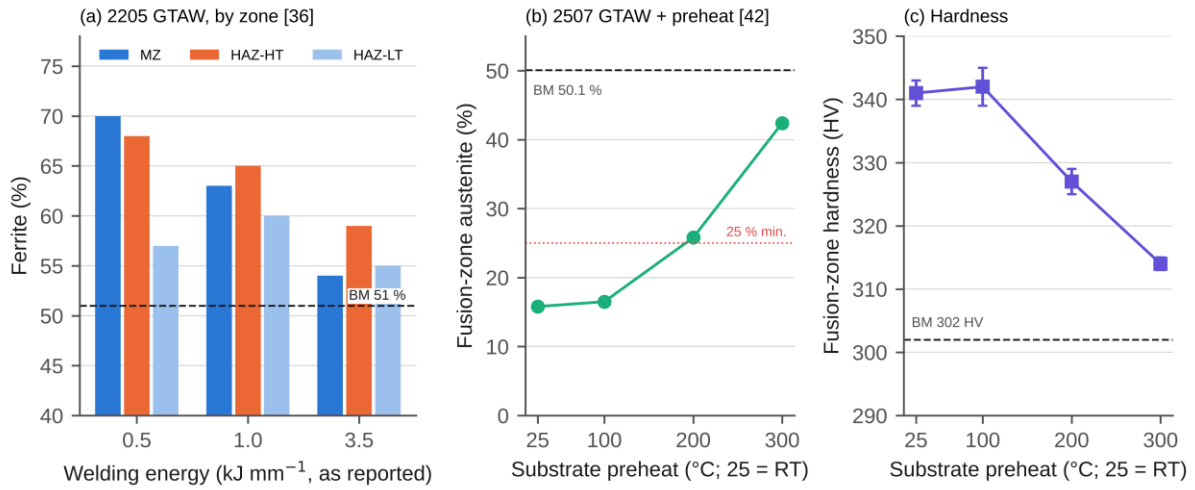


Fig. 11 Additional experimental data on thermal control of phase balance: (a) ferrite in the molten zone (MZ), high-temperature HAZ (HAZ-HT) and low-temperature HAZ (HAZ-LT) of 2205 GTAW joints at welding energies of 0.5, 1.0 and 3.5 kJ mm^{-1} (as reported) [36]; (b) fusion-zone austenite and (c) fusion-zone microhardness (mean ± standard deviation) of autogenous GTAW UNS S32750 welds made at room temperature and with substrate preheats of 100, 200 and 300 °C [42]. Dashed lines show base-metal values; the dotted line in (b) marks the 25 % minimum austenite cited by the authors. Replotted by the authors from the reported data

3.3.3 Shielding and backing gas

For GTAW, argon with 2–5 % N_2 is now the standard shielding gas for super duplex steels [4,41]. For GMAW the choice is more complex because the arc must remain stable with a consumable electrode. The guidelines indicate shielding gases ranging from pure argon to about 70 % Ar with additions of He, N_2, O_2 and CO_2, flow rates of 12–16 L min^{-1} for 1.0–1.6 mm wire, and the exclusion of hydrogen from both shielding and backing gases because of the risk of hydrogen embrittlement of ferrite [4]. The gas affects the process in three ways: arc physics and bead shape, nitrogen balance, and oxygen pick-up [19,26].

Helium increases arc voltage and heat transfer and improves wetting, and is therefore commonly combined with argon (for example, Ar–30 % He) in pulsed GMAW of super duplex steels [6,19]. Small additions of CO_2 or O_2 stabilise the cathode spot but oxidise the weld pool. Valiente Bermejo et al. [25] compared several shielding gases for GMAW and other processes on duplex and super duplex grades and showed that gas composition influenced arc behaviour, weld geometry and weld-metal properties. Zhang et al. [27] reported that shielding-gas composition altered the microstructure and properties of GMAW 2205 joints. Sathiya et al. [94] showed similar effects of shielding gases in duplex steel welds. The clearest evidence of the effect of oxidising gas on corrosion comes from WAAM, which uses the same arc: Akbarzadeh Chiniforoush et al. [28] compared pure argon with Ar–2 % O_2

for GMAW-based deposition of a duplex steel and found that oxygen pick-up of about 0.1 % generated complex oxide inclusions, more γ_2 and IGA, a thinner passive film (14.0 versus 87.3 nm) and a corrosion current density about three times higher. Inclusion-driven pitting has also been documented in WAAM super duplex [95,96].

Nitrogen additions to the shielding gas offset nitrogen loss, increase austenite and improve pitting resistance [62,97,98]. Zhang et al. [97] showed that N_2 in the shielding gas increased the austenite fraction and reduced the selective corrosion of ferrite in duplex weld joints. Kim et al. [99] reported a similar benefit for hyper duplex welds. Rodriguez-Vargas et al. [98] confirmed the effect for GTAW of 2205. In GMAW, however, the nitrogen fraction must be limited because excessive N_2 destabilises the arc and promotes porosity; most studies therefore use 1–3 % N_2, often with He [25,62]. Videira et al. [43] demonstrated the magnitude of the effect for hybrid GTAW–laser welding of UNS S32750: welding in a nitrogen atmosphere increased fusion-zone austenite from 11.1 to 34.4 % at 20 A and from 15.8 to 51.3 % at 40 A arc current, and the CPT rose from 37 to 67 °C and from 45 to 74 °C, respectively (Fig. 7b).

Backing (root purge) gas is equally important because the root is the surface exposed to the process medium in pipes. Pure N_2 or Ar–N_2 backing is preferred [4,6]. Westin et al. [48] examined backing gases containing nitrogen and hydrogen for super duplex welds and showed that the backing-gas composition alters the microstructure and properties of the root surface; the fabrication guidelines nevertheless advise against hydrogen in either shielding or backing gas for duplex grades [4].

3.3.4 Filler metal and dilution

The standard GMAW consumable for UNS S32750 is ER2594 (EN ISO 14343 G 25 9 4 N L), with about 25 % Cr, 9–10 % Ni, 4 % Mo and 0.25 % N [4,6]. Nickel over-alloying raises the austenite fraction of the as-welded metal. Muthupandi et al. [53] showed for standard duplex welds that weld-metal chemistry, particularly Ni and N, has a larger effect on phase balance than heat input, a conclusion supported for super duplex steels by laser and plasma welding experiments with nickel additions [56,100]. The optimum nickel level is nevertheless a balance: nickel improves austenite formation and has been shown to influence weld-metal toughness [101], but by reducing the ferrite fraction it also concentrates Cr and Mo in the remaining ferrite, which can favour σ during reheating [34,59]. Dandekar et al. [35] compared ER2594 and ER2595 consumables in SMAW of UNS S32750 and found 68 % ferrite in the cap and 55 % in the root pass for ER2594, with harder weld metal for ER2595.

Amiri et al. [44] evaluated several filler rods for GTAW of S32750 and showed that the choice affected phase balance, strength and pitting resistance.

Dilution is a particular issue in root passes and in dissimilar joints. Autogenous or highly diluted root passes are leaner in Ni and N than the filler and therefore more ferritic [4,15]. In dissimilar joints with Ni-base alloys or carbon steels, the filler metal must also avoid hard martensitic or fully austenitic zones [102,103]. Kangazian and Shamanian [102] examined the effect of pulsed current on the microstructure, mechanical properties and corrosion behaviour of Ni-alloy/super duplex dissimilar welds, showing that current waveform is a useful control variable beyond GMAW.

3.3.5 Root pass and joint design

Because GMAW root passes are prone to lack of fusion, a GTAW root followed by GMAW fill and cap passes is common for pipe [4,17]. Arun et al. [17] compared multipass arc welding techniques for 12 mm super duplex plate and found that the process combination influenced the microstructure, mechanical properties and corrosion resistance of the joint. Root-pass techniques for GMAW of duplex plate, including modified short-circuit processes, remain an active research topic. The IMOA guidelines recommend that the arc energy of the second and subsequent passes be lower than that of the root (around 75 %) to limit reheating of the root, and that copper backing bars be avoided because of copper contamination and over-rapid quenching [4,6].

3.3.6 Advanced and data-driven parameter selection

Statistical design and soft-computing methods are increasingly used to select GMAW parameters. Payares-Asprino [20] used artificial neural networks to predict the mechanical properties of robotic GMAW 2205 welds from welding variables. Response-surface and parametric studies have been applied to super duplex WAAM [24,71]. Prunbauer et al. [93] showed how a material model can feed welding simulations of SAF 2507. These approaches have not yet been coupled with microstructure-kinetics models for σ and Cr_2N in GMAW of UNS S32750, which is a clear opportunity (Section 4.4). Gaussian process regression and Bayesian optimisation, which are particularly suited to the small, noisy data sets typical of welding experiments, are reviewed separately in Section 4.3.

3.4 Microstructure across the weld zones

The microstructure of a GMAW UNS S32750 joint can be divided into the weld metal, the HT-HAZ, the low-temperature HAZ (LT-HAZ) and the unaffected base metal (Fig. 9a). The weld metal of a single pass consists of columnar ferrite grains with GBA, WA and IGA

[35,45]. Han et al. [45] found three austenite morphologies in the weld centre but only two in the cap and root, which they related to different cooling rates. Texture analysis has shown that austenite and ferrite in the fusion zone obey the Kurdjumov–Sachs orientation relationship [35].

The HT-HAZ is heated close to the solidus, so the austenite dissolves almost completely and ferrite grains coarsen; on cooling, the austenite reforms only partly. This zone usually has the highest ferrite content in the joint: 61–65 % in the 33 mm joints of Valiente Bermejo et al., about 10 % more than the corresponding weld metal (Fig. 10a) [6]. In the 2205 GTAW joints of Pereira et al. [36], the HT-HAZ contained 68, 65 and 59 % ferrite at welding energies of 0.5, 1.0 and 3.5 kJ mm^{-1}, compared with 57, 60 and 55 % in the LT-HAZ and 51 % in the base metal (Fig. 11a); at the highest energy the HT-HAZ, rather than the molten zone, was the most ferritic region. Westin and Wessman [91] reviewed the characteristics of high-temperature HAZs in duplex stainless steels, including the roles of peak temperature, time above the ferrite solvus and nitrogen loss. Higelin et al. [104] demonstrated that the HT-HAZ ferrite content can be controlled through the base-metal composition. The HT-HAZ is also where Cr_2N precipitates most frequently [6,45,52]. The LT-HAZ is heated into the intermetallic range but not into the ferrite field, so it can contain σ, χ and nitrides if the time at temperature is long enough, especially when reheated [6].

In multipass welds, the reheated weld metal shows coarsened primary austenite, γ_2 and, near passes reheated many times, σ [6,47,69]. Tavares et al. [69] characterised the microstructure, chemical composition, corrosion resistance and toughness of a multipass UNS S32750 joint, emphasising the role of the reheating history. The root, which is reheated by all subsequent passes, is therefore often the critical location despite being deposited first.

3.5 Mechanical properties

3.5.1 Hardness and tensile behaviour

Properly welded UNS S32750 joints generally match or exceed the base-metal tensile strength (minimum 795 MPa), and tensile specimens usually fracture in the base metal [6,36,105]. Because ferrite is harder than austenite in duplex steels, hardness rises with ferrite content and with nitride or σ precipitation [18,35,42]. Weld-metal hardness of about 300–340 HV is typical, and offshore standards such as DNV-OS-F101 limit hardness to 350 HV [82]. Paulraj and Garg [41] found that the mechanical properties of DSS and SDSS GTAW pipe welds were better at the lower end of the 0.75–1.25 kJ mm^{-1} range studied, and that higher nitrogen in the shielding and purging gas (Ar + 5 % N_2 versus Ar + 2 % N_2) improved them.

Zhang et al. [106] reported that short heat treatments of SAF 2507 welds changed their tensile properties through the evolution of γ_2 and intermetallics.

3.5.2 Impact toughness

Impact toughness is the property most sensitive to σ. NORSOK M-601 requires an average of at least 27 J at −46 °C for super duplex weld metal and HAZ [6,107]. The GMAW and SAW joints of Valiente Bermejo et al. [6] reached 72–253 J at −46 °C and 141–309 J at room temperature, well above this requirement, even with higher-than-recommended arc energy for SAW. Devendranath Ramkumar et al. [105] characterised the weld strength and impact toughness of multipass UNS S32750 weldments and related them to the weld-metal microstructure. Hosseini et al. [10] showed that the morphology of σ, as well as its fraction, governs the loss of toughness. Vahman et al. [108] examined how welding heat input affects the structure–property relationship of a new super duplex grade.

3.5.3 Fatigue and other properties

Fatigue data for GMAW super duplex joints are scarce. Vucko et al. [109] showed that the fatigue behaviour of super duplex steel in natural seawater under cathodic protection depends on the applied potential, which is relevant to welded subsea components. Wear and tribological behaviour have been studied mainly for friction-stir-processed and WAAM super duplex [70,110].

3.6 Corrosion performance

3.6.1 Pitting corrosion and critical pitting temperature

Pitting corrosion is the principal degradation mode for welded super duplex steels in chloride service, and it is controlled by the weakest phase or the most depleted local region [32,111,112]. Perren et al. [111,112] used microelectrochemical techniques to show that, in precipitation-free super duplex steel, pitting resistance is set by the phase with the lower PREN, and that σ and Cr_2N introduce depleted zones that initiate pits at much lower potentials. Ha et al. [58,113] demonstrated that pitting resistance of UNS S32750 and 2205 depends on the phase fraction because the partitioning of Cr, Mo and N changes with it. Kang and Lee [114] correlated pitting resistance of duplex welds with the austenite–ferrite ratio.

Compiled CPT data are listed in Table 5, which separates chemical immersion tests (ASTM G48) from electrochemical tests (ASTM G150 and related potentiostatic methods), and are plotted in Figs. 7b and 7c, where the two groups are distinguished by symbol. The distinction matters because immersion CPTs are obtained in acidified ferric chloride at fixed temperature steps, whereas electrochemical CPTs are defined by a current-density threshold

626 during a temperature ramp at a fixed potential; the two give systematically different values for
627 the same material [6,38,39]. In the electrochemical group, base-metal CPTs of 84 ± 2 °C [6]
628 and 92 °C [43] were reported for UNS S32750, but Ketabi et al. [16] obtained only 58 °C for
629 their pipe base metal and showed that the measured CPT varied between 28 and 58 °C for the
630 same material depending on solution, potential and surface preparation. Arc welds gave 45–
631 54 °C for multipass GTAW [16] and 64.7–70.9 °C for SAW, the latter measured with a
632 modified time setting that the authors note is not strictly a CPT [6]; laser and hybrid GTAW–
633 laser welds gave 26–74 °C depending on austenite content [43]. In the data of Videira et al.
634 [43], CPT and fusion-zone austenite are almost linearly related (r = 0.97, Fig. 7b). In the
635 immersion group, ASTM G48 Method E gave 60 °C for the pulsed GMAW joint and 45 and
636 55 °C for the SAW joints made at recommended and high arc energy [6]; notably, the SAW
637 joint made at higher arc energy had the higher CPT by both methods. ASTM G48 Method A,
638 a fixed-temperature weight-loss test, does not yield a CPT and is used as a pass/fail criterion,
639 for example for linear friction welds of UNS S32760 [82]. Because of this method sensitivity,
640 weld CPTs should be judged against the base-metal CPT measured with the same method, and
641 values from the two groups should not be pooled.

642 **Table 5** Compiled pitting corrosion data for UNS S32750 base metal and welds, grouped by test method: (a) chemical immersion tests (ASTM G48)
643 and (b) electrochemical tests (ASTM G150 and related potentiostatic methods)

Ref.	Process / condition	Test method	Base metal CPT (°C)	Weld CPT (°C)	Remarks
(a) Immersion pitting tests in ferric chloride (ASTM G48) [38]					
[6]	Pulsed GMAW, 33 mm (GM-R), arc energy 1.18–1.58 kJ mm^{-1}	G48 Method E	n.r. (G48)	60	Highest G48E CPT of the three 33 mm weldments
[6]	SAW, 33 mm, recommended arc energy 1.2–1.5 kJ mm^{-1} (SA-R)	G48 Method E	n.r. (G48)	45	17 passes
[6]	SAW, 33 mm, high arc energy 2.0–2.3 kJ mm^{-1} (SA-H)	G48 Method E	n.r. (G48)	55	8 passes; higher arc energy, higher CPT
[82]	Linear friction weld, UNS S32760	G48 Method A (fixed temperature, weight loss)	–	No pitting (pass)	Pass/fail test; no CPT obtained
(b) Electrochemical critical pitting temperature (ASTM G150 and related potentiostatic methods) [39]					
[6]	SAW, 33 mm, SA-R and SA-H	G150, modified time setting*	84 ± 2	64.7 (SA-R); 70.9 (SA-H)	Pitting initiated in WM (SA-R) and HAZ (SA-H). *Not strictly a CPT according to the authors
[16]	Multipass GTAW, 8.2 mm pipe, 105 / 130 / 155 / 180 A	G150 (1 °C min^{-1}; 100 µA cm^{-2} threshold)	58	54 / 51 / 47 / 45	Same base metal gave 28–58 °C under different test conditions
[43]	Laser welds in Ar or N_2 (LA, LN)	G150	92	26 / 27	FZ austenite 7.3–7.5 %
[43]	Hybrid GTAW–laser, Ar (20 A and 40 A arc)	G150	92	37 / 45	FZ austenite 11.1–15.8 %
[43]	Hybrid GTAW–laser, N_2 atmosphere (20 A and 40 A arc)	G150	92	67 / 74	FZ austenite 34.4–51.3 %

644 n.r. = not reported. CPTs from immersion and electrochemical methods are not directly comparable and must be judged against a base-metal value measured by the same method [16]. The data of
645 Videira et al. are plotted in Fig. 7b.

The location of pit initiation reflects the microstructure. Pits initiate in the ferrite of the HAZ [36,45,115], at Cr_2N-associated Cr-depleted zones [45,68], at γ_2 in reheated passes [6,66], at α/γ interfaces in low-heat-input GMAW joints [18], and at oxide inclusions in oxygen-contaminated deposits [28,95]. Hou et al. [115] clarified the initiation mechanism of pitting in the weld HAZ of a duplex steel, in which local microstructural heterogeneity of the reheated ferrite plays a central role. Zhang et al. [57] linked selective pitting in weld joints to elemental partitioning, and Shen et al. [116] showed that microstructural evolution in duplex welded joints controls both hardness and pitting.

3.6.2 Passive film behaviour

The passive film on super duplex steel is a bilayer of Cr- and Fe-oxides/hydroxides, enriched in Mo species [117,118]. Rahimi et al. [118] found differences in the passive layer on ferrite and austenite of super duplex steel. Cui et al. [117,119] showed that the passivity of 2507 depends on dissolved oxygen, pH and temperature in seawater and flue-gas condensates. Electrochemical impedance spectroscopy of different zones of a UNS S32750 weldment indicated similar passive-film structures across the joint, so the reduction in pitting resistance stems from local depletion rather than from a different film [45]. In contrast, oxidising shielding gas produced a markedly thinner and more defective passive film in GMAW-based deposits [28].

3.6.3 Intergranular and selective corrosion

Double-loop electrochemical potentiokinetic reactivation (DL-EPR) is used to assess sensitisation caused by Cr_2N, σ and χ [16,120]. Hong et al. [120] optimised the DL-EPR method for aged UNS S32750. Ketabi et al. [16] reported that the degree of sensitisation (charge ratio Qr/Qa) in GTAW UNS S32750 joints increased from 2.49 % at 105 A to 4.2, 9.0 and 10.25 % at 130, 155 and 180 A, compared with 1.55 % for the base metal, while the CPT (ASTM G150) fell from 54 to 51, 47 and 45 °C (base metal 58 °C) (Fig. 8b and (c)). The largest step occurred between 130 and 155 A: no σ or χ was found at 105 and 130 A, whereas EDS indicated probable Mo-rich χ and carbide particles in the welds made at 155 and 180 A, and the authors recommended 105–130 A (arc energy 0.78–0.99 kJ mm^{-1}; net about 0.47–0.59 kJ mm^{-1}) as the optimum. In 2205 joints welded at 3.5 kJ mm^{-1}, the HAZ showed intergranular attack along α/γ interfaces in ASTM A262 practice A tests [36]. Selective corrosion of ferrite in flux-cored and multipass duplex welds has been related to elemental partitioning [76].

3.6.4 Environmentally assisted cracking and hydrogen

Super duplex steels resist chloride stress corrosion cracking better than austenitic grades, but cracks can initiate from pits and are deflected or arrested by austenite [32,121]. Song et al. [121] studied stress corrosion cracking of 2205 with simulated welding microstructures in simulated seawater at different depths. Hydrogen-induced stress cracking (HISC) under cathodic protection is a recognised failure mode for subsea super duplex components, and welds with coarse ferrite and low austenite spacing are particularly susceptible [32,122]. Meinhardt et al. [122] demonstrated hydrogen embrittlement of FSW super duplex joints under cathodic protection. This is one reason why hydrogen-containing shielding or backing gases are excluded for duplex steels [4,48]. Liu et al. [32] noted that α/γ phase boundaries act both as hydrogen traps and as rapid diffusion paths.

3.7 Post-weld heat treatment and remediation

Solution annealing at about 1050–1125 °C followed by water quenching restores phase balance, dissolves σ and Cr_2N and recovers pitting resistance, but it is rarely practical for fabricated structures [4,50,123]. Cervo et al. [50,123] showed that the annealing temperature controls both the phase balance and the partitioning of elements in UNS S32750 welded joints, and evaluated the corresponding pitting resistance. Short heat treatments have been explored as an alternative: Zhang et al. [49,106] showed that brief heat treatments of UNS S32750 welds modify the phase balance and the γ_2 and intermetallic content, with direct consequences for pitting resistance and tensile behaviour. Similar results were found for standard duplex and laser welds [124,125]. Li et al. [126] and Shen et al. [127] showed that the solution-treatment temperature of UNS S32750 controls the ferrite proportion and precipitates and hence dual-phase corrosion. Ferrari et al. [128] showed that shielding gas and PWHT both affect the mechanical and corrosion performance of low-heat-input duplex and super duplex joints. Surface nickel or cobalt deposition before laser welding has been used to correct phase balance in UNS S32750 [129], but such approaches are not applicable to GMAW, in which Ni is supplied by the filler.

3.8 GMAW-based wire-arc additive manufacturing of super duplex stainless steel

WAAM uses GMAW or CMT to deposit hundreds of overlapping beads, so it represents an extreme case of the multipass reheating discussed in Section 3.3.2. It is, however, not simply a joint with more passes, and results from the two should be transferred with care. Hosseini et al. [21] analysed thermal cycles during WAAM of a duplex steel and related the repeated reheating of earlier layers to the resulting microstructure. Kannan et al. [22] and

Kumar and Maji [71] studied WAAM of super duplex steel and showed that deposition parameters control bead geometry, phase balance and properties. Akselsen et al. [130] reported σ formation in WAAM super duplex walls. Pant et al. [23,51] fabricated ER2594 walls with CMT, characterised their metallurgical, mechanical and corrosion behaviour, and followed the evolution of microstructure and properties under thermal ageing and solution treatment; the latter study was published in this journal. Ramkumar et al. [24] proposed a process-driven roadmap for depositing super duplex steel by WAAM. Shielding-gas chemistry is again critical: oxygen-containing gas degraded corrosion resistance [28], and inclusions governed localised corrosion [95,96]. Akbarzadeh et al. [131] found that the shielding gas influenced microstructure and mechanical properties of WAAM duplex steel. Dissimilar SDSS 2507/Inconel 718 structures have also been built by CMT-based deposition [70]. Lessons from WAAM, particularly on thermal-cycle control, interlayer temperature and gas purity, are directly transferable to thick-section multipass GMAW, and vice versa.

The thermal boundary conditions in WAAM differ from those in multipass joint welding in three important ways. First, a thin wall conducts heat mainly downwards towards the substrate, so heat flow becomes essentially two-dimensional as the wall grows, whereas the root and fill passes of a thick butt joint are cooled three-dimensionally into the surrounding plate [21,132]. Second, because the cross-section available for conduction is small and the distance from the substrate increases with every layer, heat accumulates: unless the interlayer temperature is controlled by dwell time or active cooling, each new layer is deposited onto hotter material, cooling slows with build height, and the microstructure and phase balance vary along the wall [21,33]. Third, each volume of a wall is reheated by many more subsequent layers than any bead in a welded joint, often with peak temperatures in the 600–1000 °C range, so the cumulative time in the intermetallic range can be far longer than in welding; σ has been reported in super duplex WAAM walls [130]. One practical consequence is that WAAM deposits of duplex grades tend to be more austenitic than arc welds made with the same wire. Akbarzadeh Chiniforoush et al. [28] found more austenite than ferrite in both of their 2209 walls, whereas the GMAW weld-metal ferrite contents compiled in the same study for 2209 wire on 2205 plate ranged from about 48 % to more than 80 %; they concluded that results from conventional welding cannot be applied directly to WAAM without adaptation. Conversely, WAAM data on long-term reheating, interlayer-temperature control and gas purity are valuable for thick-section multipass GMAW, provided the different heat-flow geometry is taken into account. In the same study, changing from Ar–2 % O_2 to pure argon (20 L min^{-1}) lowered the corrosion current density from 49 to 13 μA cm^{-2}, raised the

corrosion potential from −69 to −30 mV and increased the estimated passive-film thickness from 14.0 to 87.3 nm [28].

3.9 Comparative evidence from other processes

Studies on other processes help to isolate mechanisms that also operate in GMAW. Laser and EBW welds of UNS S32750 show that fast cooling produces ferrite-rich fusion zones with nitrides [54,79,80,133], and that adding nitrogen, nickel or a second heat source corrects this [43,56,74]. Wang et al. [78] investigated microstructure evolution and the mechanical and corrosion properties of keyhole plasma arc welded SAF 2507. FSW of SAF 2507 and UNS S32760 avoids solidification but can still produce Cr_2N in the stir zone [68,81], while linear friction welding of UNS S32760 produced defect-free joints with balanced phases and no pitting in ASTM G48A tests [82]. Dissimilar welding of super duplex steel to pipeline steels and Ni alloys requires careful choice of filler metal and heat input [103,134,135]. Overall, these studies confirm that the governing variables in all fusion processes are cooling time, nitrogen balance and reheating, so the conclusions of this review apply broadly while the parameter values differ by process.

4 Discussion

4.1 An integrated process–microstructure–property framework for GMAW of UNS S32750

The evidence reviewed in Section 3 can be condensed into three controlling quantities, each linked to a distinct set of GMAW variables (Fig. 1, Table 6).

Table 6 Evidence-based recommended practice for GMAW of UNS S32750, with the controlling quantity each variable acts upon

Variable	Recommended practice	Controlling quantity affected	Supporting references
Transfer mode	Pulsed spray for fill and cap; GTAW or controlled short-circuit root in pipe	Cooling time; heat per pass	[4,6,17]
Arc energy	0.3–1.5 kJ mm^{-1} (guideline, $\eta = 1$); up to ≈1.6 kJ mm^{-1} pulsed GMAW demonstrated for 33 mm plate; avoid very low values in thin sections. Values >1.5 kJ mm^{-1} (SAW up to 2.3 kJ mm^{-1}) apply only to heavy-section (>30 mm) multipass joints†	Cooling time vs time at 600–1000 °C	[4,6,16]
Interpass temperature	≤100 °C (guideline). Values >100 °C (up to 180 °C) apply only to heavy-section (>30 mm) multipass joints and require procedure qualification†	Cumulative time at 600–1000 °C	[4,6,41]
Pass sequence	Fill/cap passes ≈75 % of root arc energy; minimise number of reheats of root	Cumulative reheating	[4,47,87]
Filler metal	ER2594 (Ni over-alloyed); avoid autogenous or highly diluted roots	Ni and N in weld pool	[4,35,44,53]
Shielding gas	Ar–He with small N_2 additions; avoid or minimise CO_2/O_2; no H_2; 12–16 L min^{-1}	N retention; O pick-up	[4,25,28,62]
Backing gas	N_2 or Ar–N_2; no H_2	Root N balance and oxidation	[4,48]
Preheat	Not normally required; can raise austenite in thin, fast-cooled welds	Cooling time	[4,42]
Acceptance testing	Ferrite 30–70 %, ≥27 J at −46 °C, ≤350 HV; G48 and G150 CPT with base-metal reference	Verification	[38,39,82,107,136]

Recommendations synthesise guideline values and the cited experimental evidence; they do not replace procedure qualification. †Caveat: parameters above 1.5 kJ mm^{-1} arc energy and 100 °C interpass temperature were qualified only for 33 mm plate [6], where cooling remained three-dimensional and the number of passes was about halved; applied to thinner sections or other joint designs they may cause σ-phase embrittlement.

The first is the cooling time through roughly 1200–800 °C, which governs how much primary austenite forms in the weld metal and the HT-HAZ. It is set by arc energy, plate thickness (two- versus three-dimensional heat flow), interpass temperature and preheat [4,6,42]. Short cooling times give ferrite contents above 70 % and quenched-in Cr_2N, with low toughness and pitting at nitride-associated depleted zones [8,45,54].

The second is the nitrogen and nickel available in the weld pool, which sets the driving force for austenite formation and the PREN of the austenite. It is controlled by the filler (ER2594 over-alloyed with Ni), dilution, and the nitrogen partial pressure in the shielding and backing gases, balanced against nitrogen loss at high arc temperatures [43,53,60,62]. The CPT data in Fig. 7b show that, at least for low-heat-input processes, the austenite fraction and hence the nitrogen balance dominates pitting resistance more strongly than any other measured variable.

The third is the cumulative time that each volume of material spends in the 600–1000 °C range over the whole welding sequence, which governs σ, χ, isothermal Cr_2N and γ_2. It depends on the number and sequence of passes, the arc energy of each pass relative to the previous one, and the interpass temperature [6,16,47].

GMAW variables usually act on more than one of these quantities at the same time. Raising the arc energy, for example, lengthens the cooling time, which is beneficial, but also increases the time spent in the intermetallic range per pass, which is detrimental; at the same time, it reduces the number of passes, which is beneficial. This explains why studies report opposite trends with heat input (Fig. 7a and (c)) and why the single-pass heat input window used in most procedure specifications (0.3–1.5 kJ mm^{-1} for 2507 [4]) is a necessary, but not sufficient, control. The results of Valiente Bermejo et al. [6], in which SAW at up to 2.3 kJ mm^{-1} and 180 °C interpass met all requirements for 33 mm plate while halving the number of passes, and those of Ketabi et al. [16], in which more passes at lower current produced more secondary phases and a higher degree of sensitisation, both point to the cumulative thermal history as the more fundamental variable. A practical process window that reflects this is summarised in Fig. 12 and Table 6. An important caveat applies to this window: the conditions above 1.5 kJ mm^{-1} arc energy and 100 °C interpass temperature were qualified only for 33 mm plate in a multipass configuration [6], in which heat flow remained three-dimensional and the number of passes was roughly halved. They should not be applied to thinner sections, to single-sided pipe joints, or to joint designs with less effective heat sinking, where the same settings would lengthen the time in the 600–1000 °C range and could cause σ

embrittlement. Outside heavy sections, the guideline limits of 0.3–1.5 kJ mm^{-1} and an interpass temperature of 100 °C or less [4] remain the appropriate default.

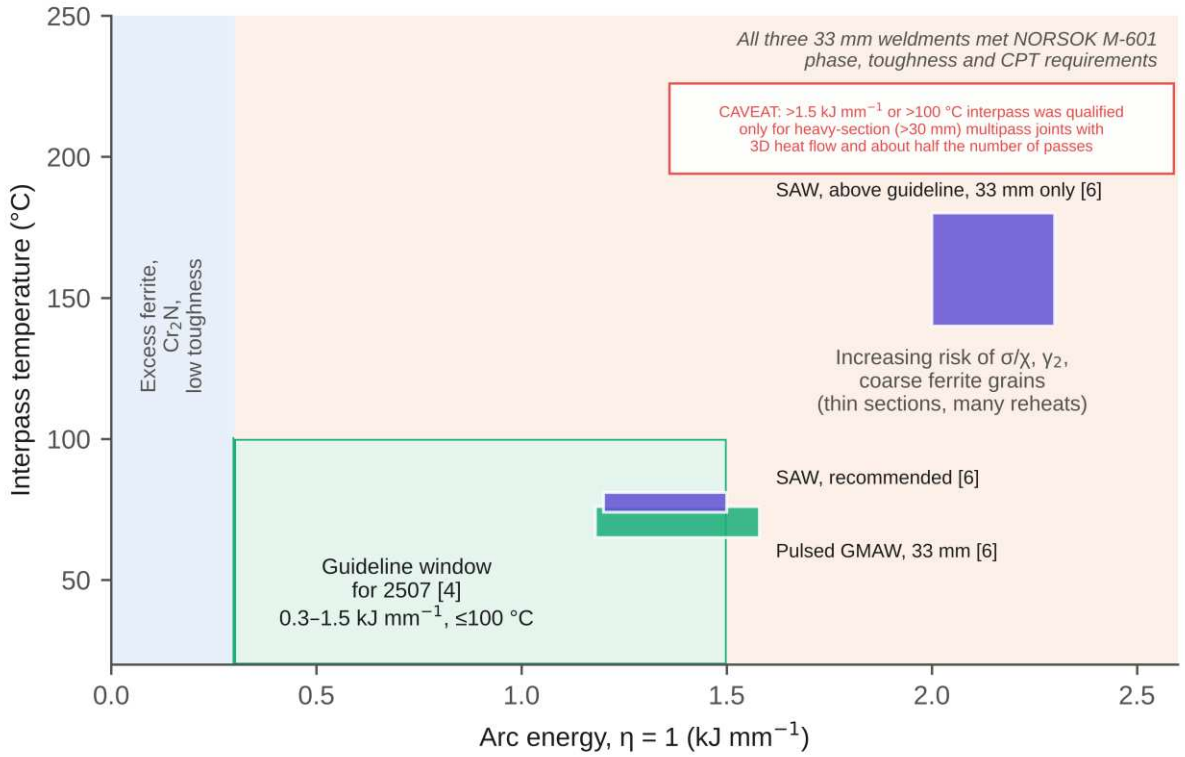


Fig. 12 Recommended process window for GMAW of UNS S32750 in terms of arc energy (η = 1, the basis of the guideline) and interpass temperature: the guideline window for 2507 [4] compared with the qualified pulsed GMAW and SAW conditions for 33 mm plate [6], all of which met NORSOK M-601 requirements [107]. Caveat: the conditions above 1.5 kJ mm^{-1} and 100 °C interpass apply strictly to heavy-section (>30 mm) multipass joints, in which cooling remains three-dimensional and the number of passes is significantly reduced; they should not be applied to thinner sections or other joint designs, where they may cause σ-phase embrittlement. Regions outside the window are annotated with the dominant metallurgical risk

4.2 Critical appraisal of the evidence base

Several limitations of the current literature affect the confidence with which parameters can be transferred between studies and to industrial practice.

First, GMAW-specific data on UNS S32750 are scarce. Much of the quantitative parameter–property evidence comes from GTAW [15,16,41,42], laser and hybrid processes [43,54] or standard and lean duplex grades welded by GMAW [18,27,36,40]. Mechanisms transfer well, but parameter values do not, because thermal efficiency, droplet superheat and nitrogen loss differ between processes. The large-thickness study of Valiente Bermejo et al. [6] and the earlier MIG/MAG study of Lopes et al. [137] are among the few that report full GMAW data for S32750.

Second, reporting is inconsistent. Many studies report heat input without specifying thermal efficiency or whether the value refers to arc energy; among the data sets compiled here, the efficiency used ranged from 0.65 to 1.0 or was not stated (Table A1), which alone can shift a reported value by more than 50 % relative to the EN 1011-1 net heat input [37]; pulsed GMAW is often reported with mean current and voltage, although instantaneous power is the physically meaningful quantity for pulsed waveforms. Interpass temperature, pass sequence and gas flow are frequently omitted. Without these values, the cumulative thermal history cannot be reconstructed.

Third, phase quantification methods vary. Point counting, image analysis of colour-etched sections, magnetic induction and EBSD give systematically different ferrite fractions, especially when fine IGA and γ_2 are present [6,16,35]. Differences of 5–10 % between studies may therefore reflect the method rather than the welding process.

Fourth, corrosion test methods are not harmonised. CPTs measured by ASTM G48 immersion and ASTM G150 potentiostatic methods are not directly comparable, and Ketabi et al. [16] showed CPTs between 28 and 58 °C for the same material depending on test solution and potential. Base-metal CPTs of 84–92 °C for UNS S32750 were obtained in two studies using ASTM G150 [6,43], while lower base-metal values reported elsewhere may reflect a different thermal history of the as-received plate [16]. Weld assessments should therefore always report the base-metal CPT measured with the same method, and compilations should keep immersion and electrochemical CPTs separate, as in Table 5.

Fifth, the role of oxygen has been underestimated. Many GMAW studies on duplex steels used Ar–CO_2 or Ar–O_2 mixtures without reporting weld-metal oxygen. The WAAM results [28,95,96] show that oxide inclusions can dominate pitting initiation, and this effect is probably present in conventional GMAW welds made with active gases.

Finally, data on hydrogen-assisted cracking, fatigue and long-term ageing of GMAW super duplex welds are very limited, although these are often the design-limiting properties in subsea service [32,109,122].

4.3 Gaussian process regression for optimising GMAW parameters: mechanical properties, microstructure and pitting resistance

The appraisal in Section 4.2 shows that the welding of UNS S32750 is governed by several interacting variables, that each experimental weld is expensive (a 33 mm joint requires 8–18 passes and up to about 55 min of arc time [6]), and that the property responses, namely ferrite fraction, secondary-phase content, toughness, hardness and CPT, are non-linear and

noisy. These are the conditions under which Gaussian process regression (GPR) and the Bayesian optimisation (BO) built on it are most useful, because they deliver accurate predictions from a few tens of experiments together with an explicit estimate of the prediction uncertainty [138–140]. This section reviews the principles of GPR, its application to welding, additive manufacturing and corrosion, and the way in which it can be used to optimise GMAW parameters for UNS S32750. The studies reviewed are summarised in Table 7.

Table 7 Summary of studies applying Gaussian process regression (GPR) and GP-based Bayesian optimisation (BO) to welding, additive manufacturing and corrosion, with two non-GPR machine-learning studies on super duplex deposition and pitting for comparison

Ref.	Process / material	Inputs	Outputs	Model	Data	Reported performance
(a) Arc welding						
[141]	GTAW	Welding parameters (e.g. current)	Weld performance indices	GPR + BO	n.r.	Optimum found with fewer experiments than conventional methods
[142]	GTAW	Welding parameters	Bead geometry	GPR, cross-validated	n.r.	Predictions matched measured bead geometry
[143]	Hybrid-tandem GMAW	Leading current 360–440 A, leading voltage 32–40 V, trailing current 320–400 A (ANOVA-selected from 7)	7 penetration, leg-length and convexity measures	ARD squared-exponential GPR + SQP	5 levels × 5 repeats	Validation error 2.28–10.43 %; 1.9 m min^{-1}
[144]	CMT wire-arc AM	Wire feed 2.6–5.2 m min^{-1}, travel speed 0.25–1.0 m min^{-1}, interpass time 0–60 s	Effective-area ratio, height difference, deposit angle	ARD squared-exponential GPR + SQP	12 conditions × 3	Error 0.1–4.3 %; buy-to-fly 0.49 → 0.43
(b) Solid-state and laser welding						
[145]	Friction stir welding, AA6082	Rotational speed, feed rate	Ultimate tensile strength	GPR (RBF, PUK) vs SVM, MLR	25 (19 train / 6 test)	GPR-RBF: r = 0.97, RMSE 5.94 MPa (MLR 22.4 MPa)
[146]	Friction stir welding	Surface topography, process signals, process parameters	Ultimate tensile strength	GPR; RBF, RQ, Matérn 5/2, additive, spectral-mixture kernels	54 welds, 216 specimens	Pearson r up to 0.99; better than MLR
[147,148]	Deep-penetration laser welding	Laser power, speed, core/ring power share	Capillary depth, porosity, seam elevation, undercut	Matérn 5/2 GP + expected improvement	8 Sobol + 100 BO steps	First acceptable weld at step 24; 7 acceptable welds; up to 20.6 m min^{-1}
[149]	Laser welding, polishing, cutting	Power, speed and process-specific settings	Capillary depth and defects; roughness; burr	GP-based BO (Ax)	24 welds to best result	Capillary depth 1.54 mm at 8 kW and 30.7 m min^{-1}
(c) Additive manufacturing and corrosion						
[150]	Laser powder bed fusion, 316L	6 parameters (power, speed, hatch, scan angle, layer time, gas speed)	Hardness, porosity	Matérn GP per objective, multi-objective BO	57 initial specimens	3 Pareto points in ≈6 iterations; 224–235 HV, porosity 0.2–0.37 %
[151]	Metal additive manufacturing	Process parameters, location	Porosity	Spatial GP model	n.r.	Porosity predicted from process conditions
[152]	Fe–Cr alloys in NH_3	Temperature, NH_3 concentration, composition	Corrosion mass gain	GPR + BO	n.r.	$R^2 > 0.95$
(d) Non-GPR comparison studies						
[153]	Super duplex wire-arc AM	Voltage, wire feed, travel speed, gas flow	Deposition efficiency, surface height	ANN, ANFIS + NSGA-II	75 runs (CCD)	ANFIS deviation 6.1 % / 14.9 %; ≈70 % austenite
[154]	Austenitic stainless steels	Composition, test conditions, physical descriptors	CPT	GBDT, random forest, symbolic regression	123 alloys	R^2 0.974, RMSE ≈4.6 °C

n.r. = not reported in the information extracted; ARD = automatic relevance determination; SQP = sequential quadratic programming; RBF = radial basis function; PUK = Pearson VII universal kernel; RQ = rational quadratic; MLR = multiple linear regression; CCD = central composite design. No GPR study on GMAW of super duplex stainless steel was identified.

4.3.1 Principles of Gaussian process regression and Bayesian optimisation

A Gaussian process is a distribution over functions in which any finite set of function values has a joint Gaussian distribution. In GPR, the unknown relationship $y = f(x) + \varepsilon$ between a vector of process inputs x (for example net heat input, interpass temperature, shielding-gas nitrogen content and travel speed) and a measured response y (for example weld-metal ferrite or CPT) is given the prior $f(x) \sim GP(m(x), k(x, x'))$, where m(x) is a mean function, usually a constant, $k(x, x')$ is a covariance (kernel) function and ε is Gaussian measurement noise with variance σ_n^2 [138,139]. The kernel encodes assumptions about smoothness. The squared-exponential kernel with automatic relevance determination (ARD), $k(x, x') = \sigma_f^2 \exp[-\tfrac{1}{2} \Sigma_d (x_d - x'_d)^2/\ell_d^2]$, assigns each input d its own length-scale ℓ_d, so that inputs with short length-scales are identified as influential; the Matérn 5/2 kernel relaxes the assumption of infinite smoothness and is often preferred for physical processes [138,155]. Given n training welds with inputs X and responses y, the predictive distribution at a new parameter set x* is Gaussian, with mean $\mu(x^*) = k^{*T}(K + \sigma_n^2 I)^{-1} y$ and variance $\sigma^2(x^*) = k(x^*, x^*) - k^{*T}(K + \sigma_n^2 I)^{-1} k^*$, where K is the n × n covariance matrix of the training inputs and k* the vector of covariances between x* and the training inputs. The hyperparameters σ_f, ℓ_d and σ_n are obtained by maximising the log marginal likelihood, which automatically balances data fit against model complexity [138,140].

GPR has its roots in the kriging-based design and analysis of computer experiments [156] and in the Bayesian calibration of computer models, in which a GP is used both to emulate a simulation and to represent the discrepancy between simulation and experiment [157]. The second idea is directly relevant to welding, where numerical thermal models [93] can be calibrated against a small number of instrumented welds. Because GPR gives both a mean and a variance, it can drive sequential experimentation. In BO, an acquisition function decides which weld to make next. Expected improvement, $EI(x) = E[\max(0, f(x) - f^+)]$, where f^+ is the best result so far, rewards both a high predicted mean and a high uncertainty [158]; the upper confidence bound, $\mu(x) + \beta^{1/2}\sigma(x)$, offers explicit control of the balance between exploitation and exploration, with proven convergence guarantees [159]. Comprehensive reviews of BO, including constrained, multi-objective and batch variants, are given by Shahriari et al. [160], Garnett [161] and Wang et al. [162].

4.3.2 Gaussian process regression in welding and related processes

The first applications of GPR to arc welding were made for GTAW. Sterling et al. [141] modelled the relationship between welding parameters and weld performance indices with

GPR and combined it with a Bayesian optimisation algorithm, showing that optimal parameters could be found with fewer experiments than with conventional methods. Dong et al. [142] used GPR with cross-validation to predict the bead geometry of GTAW welds from the welding parameters, and highlighted its robustness to the noise and uncertainty of the arc process.

For GMAW, the most relevant study is that of Kim et al. [143] on hybrid-tandem GMAW. Analysis of variance was first used to reduce seven candidate parameters to the three most influential (leading current 360–440 A, leading voltage 32–40 V and trailing current 320–400 A); an ARD squared-exponential GPR was then trained to predict seven geometric quality measures, including vertical and horizontal penetration, penetration beyond the root, leg lengths and convexity, and was coupled with sequential quadratic programming to find the optimum. The predictions agreed with validation welds within 2.28–10.43 %, at a travel speed of 1.9 m min^{-1}. The same group applied GPR to CMT-based WAAM, using wire feed rate (2.6–5.2 m min^{-1}), travel speed (0.25–1.0 m min^{-1}) and interpass time (0–60 s) as inputs and only 12 experimental conditions with three repeats each; the optimum (about 3.10 m min^{-1}, 0.35 m min^{-1} and 58 s) was predicted within 0.1–4.3 % and improved the buy-to-fly ratio from about 0.49 to 0.43 [144]. These two studies demonstrate that GPR can identify a GMAW-type optimum from 12–25 welds, which is a realistic budget for procedure development on super duplex steel.

Mechanical properties have been modelled mainly for friction stir welding. Verma et al. [145] compared GPR, support vector machines and multiple linear regression for predicting the ultimate tensile strength of friction stir welds from 25 experiments; GPR with a radial basis function kernel performed best (correlation coefficient 0.97, root-mean-square error 5.94 MPa, compared with 22.4 MPa for linear regression). Hartl et al. [146] tested several kernels, including ARD, Matérn 5/2, additive and spectral-mixture kernels, on 54 welds and 216 tensile specimens and obtained Pearson correlation coefficients of up to 0.99 between predicted and measured strength, again clearly outperforming linear regression.

In laser welding, GP-based BO has recently become a practical tool. Haas et al. [147,148] used a Matérn 5/2 GP surrogate with an expected-improvement acquisition function to optimise deep-penetration laser welding for capillary depth, porosity, seam elevation and undercut; after 8 space-filling initial experiments, the first weld meeting all four quality criteria was found at step 24, and seven acceptable welds were obtained at speeds up to 20.6 m min^{-1}. Menold et al. [149] showed that the same generic BO tool reached the target capillary depth (1.54 mm) after 24 welding experiments and was equally applicable to

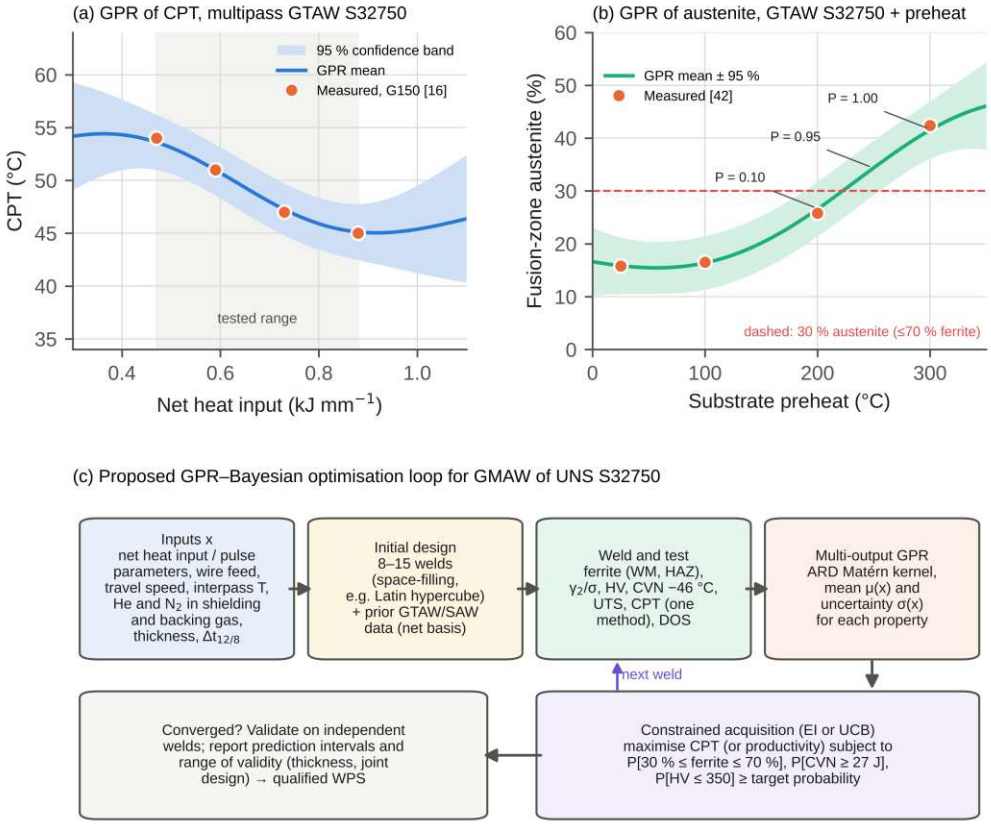
polishing and cutting. In laser powder bed fusion of 316L stainless steel, separate Matérn GP models for hardness and porosity were used in a multi-objective BO that located three Pareto-optimal parameter sets in about six iterations from 57 initial specimens, with validated hardness of 224–235 HV and porosity of 0.2–0.37 % [150]; spatial GP models have also been used to predict porosity in metal additive manufacturing [151].

4.3.3 Gaussian process regression for microstructure and corrosion targets

Applications of GPR to corrosion are fewer but growing. Itano et al. [152] used GPR to predict the corrosion mass gain of Fe–Cr alloys in ammonia from temperature, ammonia concentration and composition, reaching R^2 above 0.95, and then used BO to propose conditions and compositions expected to improve corrosion resistance. For the pitting resistance of stainless steels, data-driven models have so far relied mainly on tree-based and kernel methods: Hou et al. [154] predicted the CPT of 123 austenitic stainless steels with R^2 of 0.974 and an RMSE of about 4.6 °C from three physically interpretable descriptors. For super duplex steel, Kumar et al. [153] modelled the deposition efficiency and surface height of WAAM deposits with artificial neural networks and an adaptive neuro-fuzzy inference system (mean absolute deviations of 6.1 % and 14.9 %) and optimised them with a genetic algorithm, obtaining deposits with about 70 % austenite; Payares-Asprino [20] used neural networks for robotic GMAW of 2205. To the authors' knowledge, no study has yet applied GPR or GP-based BO to the microstructure, mechanical properties or pitting resistance of GMAW welds in UNS S32750 or any other super duplex grade. This is a significant gap, because the uncertainty estimates of GPR are particularly valuable when the acceptance criteria are two-sided (30–70 % ferrite) or safety-related (minimum toughness and CPT).

To illustrate the potential, GPR models were fitted by the present authors to two of the experimental data sets reviewed in Section 3 (Fig. 13). For the multipass GTAW data of Ketabi et al. [16], a GPR model of CPT versus net heat input reproduces the measured decrease from 54 to 45 °C and shows how the 95 % confidence band widens outside the tested range, which is exactly the information needed to decide where the next weld should be made (Fig. 13a). For the preheat data of Da Cruz Junior et al. [42], the posterior distribution of fusion-zone austenite can be converted into the probability that a given preheat temperature satisfies the NORSOK M-601 limit of at least 30 % austenite (that is, at most 70 % ferrite) [107] (Fig. 13b). In this illustration, the probability of meeting the limit is only about 0.1 at a preheat of 200 °C but about 0.95 at 250 °C, so the model points directly to the region in which the next experiment is most informative. With only four data points each, these models are

illustrative rather than predictive, but they show how constraint satisfaction can be expressed probabilistically.



Panels (a) and (b): illustrative GPR fits by the present authors (RBF kernel; noise SD fixed at 1 °C and 2 %; four data points each); P = probability of ≥30 % austenite. Not validated predictive models.

Fig. 13 Gaussian process regression (GPR) applied to published welding data and a proposed optimisation framework: (a) GPR model of critical pitting temperature (ASTM G150) versus net heat input for multipass GTAW of UNS S32750 [16], showing the posterior mean and 95 % confidence band, which widens outside the tested range; (b) GPR model of fusion-zone austenite versus substrate preheat for GTAW of UNS S32750 [42], annotated with the posterior probability P of meeting the NORSOK M-601 limit of at least 30 % austenite [107]; (c) proposed GPR–Bayesian optimisation loop for GMAW of UNS S32750, combining a space-filling initial design, multi-output GPR with an automatic-relevance-determination Matérn kernel and a constrained acquisition function [138,158–160]. Panels (a) and (b) are illustrative fits made by the authors (radial-basis-function kernel, noise standard deviation fixed at 1 °C and 2 %, four data points each) and are not validated predictive models

4.3.4 A proposed GPR–Bayesian optimisation framework for GMAW of UNS S32750

Based on the evidence reviewed, a GPR–BO framework for GMAW of UNS S32750 is proposed in Fig. 13c. Its elements are as follows.

(i) Inputs. The decision variables should be those identified in Sections 3.3 and 4.1 as controlling the three governing quantities: net heat input or, for pulsed GMAW, peak and

background current, pulse frequency, wire feed speed and travel speed; interpass temperature and pass sequence; the He and N_2 contents of the shielding gas and the backing gas; and section thickness. Physics-based features such as the calculated cooling time $\Delta t_{12/8}$, the number of reheating cycles above 600 °C and the PREN of the filler can be added as inputs to improve extrapolation with small data sets, an approach that ARD kernels support by learning which inputs matter [140,155].

(ii) Outputs and constraints. The responses should include weld-metal and HAZ ferrite fraction, γ_2 and σ content, hardness, Charpy energy at −46 °C, tensile strength, CPT measured by a single specified method (ASTM G48 or G150), and the degree of sensitisation. Since the acceptance limits are mostly constraints rather than targets, constrained or multi-objective BO is appropriate: for example, maximising CPT subject to 30–70 % ferrite, at least 27 J at −46 °C and hardness of 350 HV or less, or finding the Pareto front between productivity and CPT [150,160,161].

(iii) Data strategy. An initial space-filling design of about 8–15 welds, followed by sequential BO, is consistent with the 12–25 experiments that sufficed in GMAW, WAAM and laser welding studies [143,144,148,149]. Existing data from GTAW, SAW and laser welding (Tables 4 and 5) can be used as prior knowledge through multi-fidelity or calibration approaches in which a GP represents the discrepancy between processes, as in the Kennedy–O'Hagan framework [157], provided that heat inputs are expressed on a common net basis (Table A1).

(iv) Validation and transferability. Models should be validated on independent welds, with prediction intervals reported, and their range of validity stated explicitly; as discussed in Sections 3.3.2 and 4.1, conditions qualified for 33 mm plate cannot be extrapolated to thin sections, and a GPR model trained on one thickness will signal this through a large predictive variance.

The main limitations of GPR are its computational cost for large data sets, which scales with the cube of the number of observations and is not restrictive for welding experiments, its sensitivity to the choice of kernel, and the need for consistent, well-documented input data [138,139]. The last point reinforces the need for standardised reporting of arc energy, efficiency, interpass temperature and test method identified in Section 4.2.

4.4 Knowledge gaps and future research directions

Based on this appraisal, the following directions are proposed.

(i) Thermal-history-based procedure qualification. Instead of single-pass heat input limits, procedures could specify a maximum cumulative time in the 600–1000 °C range and a minimum $\Delta t_{12/8}$ for each region of the joint, measured with thermocouples or computed by validated finite-element models [21,93]. The bead-by-bead approach developed for TIG, SMAW and WAAM [21,47,87] could be applied systematically to pulsed and CMT GMAW.

(ii) Nitrogen and oxygen management. Systematic studies of Ar–He–N_2 shielding gases with low or zero oxidising additions for pulsed GMAW of UNS S32750, with measured weld-metal N and O contents, are needed. The physical and theoretical models of Varbai and Májlinger [62] and Hosseini and Karlsson [61] provide a basis for predicting nitrogen balance.

(iii) Coupled kinetic and data-driven models. Precipitation kinetics for σ, χ and Cr_2N [8,11,12] could be coupled with thermal models and with machine-learning surrogates trained on literature and production data [20], in particular with the GPR–BO framework proposed in Section 4.3, which provides calibrated uncertainty and sequential experimental design [157,160] to predict ferrite fraction, secondary-phase fraction and CPT for a given GMAW procedure.

(iv) Advanced GMAW variants. Pulsed, CMT, twin-wire and hybrid laser–MIG or TIG–MIG processes offer independent control of deposition and heat input [72–75], but their metallurgical effects on UNS S32750 have not yet been mapped comprehensively.

(v) Standardised corrosion and hydrogen testing. Reporting the base-metal CPT with the same method, using both G48 and G150, and adding HISC and fatigue tests under cathodic protection would make results comparable and relevant to subsea applications [109,122].

(vi) WAAM qualification. GMAW-based WAAM of super duplex components is advancing quickly [23,24,51,130]; the extreme number of reheating cycles makes it a sensitive test of the thermal-history framework proposed here and a source of transferable data for multipass welding.

4.5 Conclusions

This review has examined the welding metallurgy of UNS S32750 super duplex stainless steel with particular reference to gas metal arc welding. The main conclusions are as follows.

1. The properties of welded UNS S32750 depend on three controlling quantities: the cooling time through about 1200–800 °C, which governs primary austenite formation; the nitrogen and nickel available in the weld pool; and the cumulative time spent between 600 and 1000 °C during multipass welding, which governs σ, χ, Cr_2N and γ_2.

2. Pulsed GMAW with ER2594 filler, Ar–He shielding gas without oxidising additions, nitrogen backing, an arc energy of about 1.2–1.6 kJ mm^{-1} (net heat input about 0.9–1.3 kJ mm^{-1}) and an interpass temperature of 100 °C or less produced joints in 33 mm plate that met NORSOK M-601 requirements (30–70 % ferrite, at least 27 J at −46 °C). Settings above 1.5 kJ mm^{-1} arc energy or 100 °C interpass have been qualified only for such heavy multipass sections and should not be transferred to thinner sections or other joint designs.

3. Heat input alone is not a reliable predictor of phase balance or corrosion resistance. The number of passes, section thickness, filler chemistry and gas composition shift the outcome by a similar or greater amount, which explains the apparently contradictory trends in the literature.

4. Weld-metal and HAZ pitting resistance is controlled by the weakest local region: ferrite with low PREN, Cr-depleted zones around Cr_2N, Cr- and Mo-depleted γ_2, or oxide inclusions. Electrochemical (ASTM G150) CPTs fall from 58–92 °C for the base metal to 45–71 °C for as-welded arc joints and increase almost linearly with fusion-zone austenite fraction; immersion (ASTM G48E) CPTs of 45–60 °C were obtained for 33 mm GMAW and SAW joints. Values from the two methods should not be compared directly.

5. Oxidising shielding gas additions produce oxide inclusions and thinner passive films that reduce corrosion resistance, as shown clearly in GMAW-based additive manufacturing.

6. The evidence base is limited by a scarcity of GMAW-specific studies on UNS S32750, inconsistent reporting of heat input and thermal efficiency, and non-harmonised phase quantification and corrosion test methods. Thermal-history-based procedure qualification, nitrogen and oxygen management, coupled kinetic and data-driven models, and standardised corrosion and hydrogen testing are recommended as the priorities for future work.

7. Gaussian process regression, combined with Bayesian optimisation, is well suited to the small, noisy and expensive data sets of super duplex welding: in arc, friction stir and laser welding and in wire-arc additive manufacturing it has identified optimal parameters or predicted strength from about 12–25 experiments with errors of a few per cent and with explicit prediction intervals. No GPR study on GMAW of super duplex steel has yet been published. A constrained, multi-output GPR–Bayesian optimisation framework that maximises CPT or productivity subject to 30–70 % ferrite, at least 27 J at −46 °C and 350 HV or less, using net heat input, interpass temperature, gas composition and thermal-history features as inputs, is proposed as a practical route to qualified GMAW procedures for UNS S32750.

Acknowledgements

The authors gratefully acknowledge Atmiya University, Rajkot, and L.E. College, Morbi, for providing access to library and computing resources during the preparation of this review.

Declarations

Funding

This research received no specific grant from any funding agency in the public, commercial or not-for-profit sectors.

Competing interests

The authors have no relevant financial or non-financial interests to disclose.

Ethics approval

Not applicable. This article is a review of previously published literature and does not contain any studies with human participants or animals performed by any of the authors.

Consent to participate

Not applicable.

Consent for publication

Not applicable. No figures, tables or images have been reproduced from other publications; all figures were drawn by the authors, either as original schematics or as re-plots of numerical data reported in the cited studies, and each source is cited in the corresponding caption.

Data availability

No new experimental data were generated in this study. All data analysed are taken from the published sources cited in the article.

Code availability

The Python scripts used to re-plot the literature data and to fit the illustrative Gaussian process regression models of Fig. 13.

Author contributions

Amit Bhalchandra Panchal: conceptualisation, methodology, literature search and data curation, formal analysis, visualisation, writing – original draft. Sagarkumar Indravadan Shah: conceptualisation, supervision, validation, writing – review and editing. Jinesh Bipinbhai Shah: methodology, validation, visualisation, writing – review and editing. All authors read and approved the final manuscript.

Clinical trial number:

Not applicable.

References

1. Nilsson JO (1992) Super duplex stainless steels. Mater Sci Technol 8(8):685–700. https://doi.org/10.1179/mst.1992.8.8.685
2. Francis R, Byrne G (2021) Duplex stainless steels—alloys for the 21st century. Metals 11(5):836. https://doi.org/10.3390/met11050836
3. Chai G, Kangas P (2016) Super and hyper duplex stainless steels: structures, properties and applications. Procedia Struct Integr 2:1755–1762. https://doi.org/10.1016/j.prostr.2016.06.221
4. International Molybdenum Association (IMOA) (2014) Practical guidelines for the fabrication of duplex stainless steels. 3rd ed. IMOA, London
5. Li T, Wang K, Lei Y (2024) A review of welding process for UNS S32750 super duplex stainless steel. Materials 17(21):5215. https://doi.org/10.3390/ma17215215
6. Valiente Bermejo MA, Eyzop D, Hurtig K, Karlsson L (2021) Welding of large thickness super duplex stainless steel: microstructure and properties. Metals 11(8):1184. https://doi.org/10.3390/met11081184
7. Nilsson JO, Wilson A (1993) Influence of isothermal phase transformations on toughness and pitting corrosion of super duplex stainless steel SAF 2507. Mater Sci Technol 9(7):545–554. https://doi.org/10.1179/mst.1993.9.7.545
8. Pettersson N, Pettersson RFA, Wessman S (2015) Precipitation of chromium nitrides in the super duplex stainless steel 2507. Metall Mater Trans A 46(3):1062–1072. https://doi.org/10.1007/s11661-014-2718-y
9. Chan KW, Tjong SC (2014) Effect of secondary phase precipitation on the corrosion behavior of duplex stainless steels. Materials 7(7):5268–5304. https://doi.org/10.3390/ma7075268
10. Hosseini VA, Karlsson L, Wessman S, Fuertes N (2018) Effect of sigma phase morphology on the degradation of properties in a super duplex stainless steel. Materials 11(6):933. https://doi.org/10.3390/ma11060933
11. Calliari I, Bassani P, Brunelli K, Breda M, Ramous E (2013) Effect of continuous cooling on secondary phase precipitation in the super duplex stainless steel ZERON-100. J Mater Eng Perform 22(12):3860–3866. https://doi.org/10.1007/s11665-013-0689-6

12. Byun SH, Kang N, Lee TH, Ahn SK, Lee HW, Chang WS, Cho KM (2012) Kinetics of Cr/Mo-rich precipitates formation for 25Cr-6.9Ni-3.8Mo-0.3N super duplex stainless steel. Met Mater Int 18(2):201–207. https://doi.org/10.1007/s12540-012-2001-y
13. Verma J, Taiwade RV (2017) Effect of welding processes and conditions on the microstructure, mechanical properties and corrosion resistance of duplex stainless steel weldments—a review. J Manuf Process 25:134–152. https://doi.org/10.1016/j.jmapro.2016.11.003
14. Pramanik A, Littlefair G, Basak AK (2015) Weldability of duplex stainless steel. Mater Manuf Process 30(9):1053–1068. https://doi.org/10.1080/10426914.2015.1019126
15. Devendranath Ramkumar K, Mishra D, Ganesh Raj B, Vignesh MK, Thiruvengatam G, Sudharshan SP et al (2015) Effect of optimal weld parameters in the microstructure and mechanical properties of autogeneous gas tungsten arc weldments of super-duplex stainless steel UNS S32750. Mater Des 66:356–365. https://doi.org/10.1016/j.matdes.2014.10.084
16. Ketabi M, Farzadi A, Rezaei M, Vazirain S, Sarmadi H, Araban V (2026) Optimizing GTAW parameters for superior corrosion resistance in UNS32750: a trade-off between welding current intensity and microstructural integrity. J Mater Res Technol 40:295–315. https://doi.org/10.1016/j.jmrt.2025.12.070
17. Arun D, Ramkumar KD, Vimala R (2019) Multi-pass arc welding techniques of 12 mm thick super-duplex stainless steel. J Mater Process Technol 271:126–143. https://doi.org/10.1016/j.jmatprotec.2019.03.031
18. Miranda-Pérez AF, Rodríguez-Vargas BR, Calliari I, Pezzato L (2023) Corrosion resistance of GMAW duplex stainless steels welds. Materials 16(5):1847. https://doi.org/10.3390/ma16051847
19. Mvola B, Kah P (2017) Effects of shielding gas control: welded joint properties in GMAW process optimization. Int J Adv Manuf Technol 88(9–12):2369–2387. https://doi.org/10.1007/s00170-016-8936-2
20. Payares-Asprino C (2021) Prediction of mechanical properties as a function of welding variables in robotic gas metal arc welding of duplex stainless steels SAF 2205 welds through artificial neural networks. Adv Mater Sci 21(3):75–90. https://doi.org/10.2478/adms-2021-0019
21. Hosseini VA, Högström M, Hurtig K, Valiente Bermejo MA, Stridh LE, Karlsson L (2019) Wire-arc additive manufacturing of a duplex stainless steel: thermal cycle

analysis and microstructure characterization. Weld World 63(4):975–987. https://doi.org/10.1007/s40194-019-00735-y

22. Kannan AR, Shanmugam NS, Ramkumar KD, Rajkumar V (2021) Studies on super duplex stainless steel manufactured by wire arc additive manufacturing. Trans Indian Inst Met 74(7):1673–1681. https://doi.org/10.1007/s12666-021-02257-y

23. Pant S, Kumar S, Shahi AS (2026) Metallurgical, mechanical, and corrosion behavior of wire arc additively manufactured super duplex stainless steel ER2594 wall fabricated using CMT welding. J Mater Eng Perform 35(2):1799–1814. https://doi.org/10.1007/s11665-025-11650-3

24. Ramkumar KR, Burad P, Mahey V, Yamamoto Y, Nycz A, Wallace R, Roy S (2026) Process-driven roadmap for depositing super duplex stainless steel via wire arc additive manufacturing. Int J Adv Manuf Technol 143(9–10):5203–5215. https://doi.org/10.1007/s00170-026-17788-1

25. Valiente Bermejo MA, Karlsson L, Svensson LE, Hurtig K, Rasmuson H, Frodigh M, Bengtsson P (2015) Effect of shielding gas on welding performance and properties of duplex and superduplex stainless steel welds. Weld World 59(2):239–249. https://doi.org/10.1007/s40194-014-0199-7

26. Wang LL, Lu FG, Wang HP, Murphy AB, Tang XH (2014) Effects of shielding gas composition on arc profile and molten pool dynamics in gas metal arc welding of steels. J Phys D Appl Phys 47(46):465202. https://doi.org/10.1088/0022-3727/47/46/465202

27. Zhang XY, Zha XQ, Gao LQ, Hei PH, Ren YF (2021) Influence of shielding gas on microstructure and properties of GMAW DSS2205 welded joints. Materials 14(10):2671. https://doi.org/10.3390/ma14102671

28. Akbarzadeh Chiniforoush E, Gholizadeh T, Jandaghi MR, Moverare J, Gür CH (2025) Impact of active to inert shielding gas transition on the corrosion behavior of wire arc additively manufactured duplex stainless steel. Mater Des 253:113907. https://doi.org/10.1016/j.matdes.2025.113907

29. Patra S, Agrawal A, Mandal A, Podder AS (2021) Characteristics and manufacturability of duplex stainless steel: a review. Trans Indian Inst Met 74(5):1089–1098. https://doi.org/10.1007/s12666-021-02278-7

30. Mohammed GR, Ishak M, Aqida SN, Abdulhadi HA (2017) Effects of heat input on microstructure, corrosion and mechanical characteristics of welded austenitic and duplex stainless steels: a review. Metals 7(2):39. https://doi.org/10.3390/met7020039

31. Maurya AK, Pandey C, Chhibber R (2021) Dissimilar welding of duplex stainless steel with Ni alloys: a review. Int J Press Vessels Pip 192:104439. https://doi.org/10.1016/j.ijpvp.2021.104439
32. Liu M, Du C, Liu Z, Wang L, Zhong R, Cheng X, Ao J, Duan T, Zhu Y, Li X (2023) A review on pitting corrosion and environmentally assisted cracking on duplex stainless steel. Microstructures 3:2023020. https://doi.org/10.20517/microstructures.2023.02
33. Zhang D, Liu A, Yin B, Wen P (2022) Additive manufacturing of duplex stainless steels – a critical review. J Manuf Process 73:496–517. https://doi.org/10.1016/j.jmapro.2021.11.036
34. Lippold JC, Kotecki DJ (2005) Welding metallurgy and weldability of stainless steels. John Wiley & Sons, Hoboken, NJ
35. Dandekar TR, Gupta A, Kumar R, Gaikwad AD, Khatirkar RK (2021) Evolution of microstructure and texture in UNS S32750 super duplex stainless steel weldments. Trans Indian Inst Met 74(9):2267–2283. https://doi.org/10.1007/s12666-021-02274-x
36. Pereira HB, Pimentel THC, da Silva CA, Panossian Z, de Azevedo CRF (2022) Influence of welding energy on intergranular and pitting corrosion susceptibility of UNS S32205 duplex stainless-steel joints. Mater Res 25(s1):e20210488. https://doi.org/10.1590/1980-5373-MR-2021-0488
37. European Committee for Standardization (CEN) (2009) EN 1011-1:2009. Welding – recommendations for welding of metallic materials – part 1: general guidance for arc welding. CEN, Brussels
38. ASTM International (2020) ASTM G48-11 (reapproved 2020): standard test methods for pitting and crevice corrosion resistance of stainless steels and related alloys by use of ferric chloride solution. ASTM International, West Conshohocken, PA
39. ASTM International (2013) ASTM G150-13: standard test method for electrochemical critical pitting temperature testing of stainless steels. ASTM International, West Conshohocken, PA
40. Chacón-Fernández S, Portolés García A, Romaní Labanda G (2022) Influence of parameters on the microstructure of a duplex stainless steel joint welded by a GMAW welding process. Prog Nat Sci Mater Int 32(4):415–423. https://doi.org/10.1016/j.pnsc.2022.06.003
41. Paulraj P, Garg R (2015) Effect of welding parameters on mechanical properties of GTAW of UNS S31803 and UNS S32750 weldments. Manuf Rev 2:29. https://doi.org/10.1051/mfreview/2015032

42. da Cruz Junior EJ, Ribeiro RH, Varasquim FMFA, Carvalho FO, Santiago LFF, Lemos GP, Ventrella VA, Calliari I (2026) Impact of substrate preheating on weld quality, microstructure, corrosion resistance, and mechanical properties in gas tungsten arc welding of UNS S32750 super duplex stainless steel. Materials 19(2):221. https://doi.org/10.3390/ma19020221
43. Videira AM, Mendes WR, Ventrella VA, Calliari I (2023) Increasing the corrosion resistance in the UNS S32750 super duplex steel welded joints through hybrid GTAW-laser welding and nitrogen. Materials 16(2):543. https://doi.org/10.3390/ma16020543
44. Amiri E, Ostovan F, Toozandehjani M, Shafiei E, Mohamed IF (2021) Study and selection of most appropriate filler rod for GTAW of S32750 super duplex steel joints: a comprehensive study on microstructural, mechanical and corrosion properties. Mater Chem Phys 270:124839. https://doi.org/10.1016/j.matchemphys.2021.124839
45. Han Y, Zhang Y, Jing H, Gao Z, Xu L, Zhang Z, Zhao L (2020) Microstructure and corrosion studies on different zones of super duplex stainless steel UNS S32750 weldment. Front Mater 7:251. https://doi.org/10.3389/fmats.2020.00251
46. Hosseini VA, Hurtig K, Karlsson L (2017) Effect of multipass TIG welding on the corrosion resistance and microstructure of a super duplex stainless steel. Mater Corros 68(4):405–415. https://doi.org/10.1002/maco.201609102
47. Hosseini VA, Hurtig K, Karlsson L (2020) Bead by bead study of a multipass shielded metal arc-welded super-duplex stainless steel. Weld World 64(2):283–299. https://doi.org/10.1007/s40194-019-00829-7
48. Westin EM, Johansson MM, Bylund LÅ, Pettersson RFA (2014) Effect on microstructure and properties of super duplex stainless steel welds when using backing gas containing nitrogen and hydrogen. Weld World 58(3):347–354. https://doi.org/10.1007/s40194-014-0120-4
49. Zhang Z, Zhao H, Zhang H, Hu J, Jin J (2017) Microstructure evolution and pitting corrosion behavior of UNS S32750 super duplex stainless steel welds after short-time heat treatment. Corros Sci 121:22–31. https://doi.org/10.1016/j.corsci.2017.02.006
50. Cervo R, Ferro P, Tiziani A, Zucchi F (2010) Annealing temperature effects on superduplex stainless steel UNS S32750 welded joints. II: pitting corrosion resistance evaluation. J Mater Sci 45(16):4378–4389. https://doi.org/10.1007/s10853-010-4311-0
51. Pant S, Kumar S, Shahi AS (2026) Wire arc additively manufactured super duplex stainless steel: microstructural and property evolution under thermal aging and solution

treatment. Can Metall Q 65(3):2665–2680. https://doi.org/10.1080/00084433.2025.2565506
52. Ramirez AJ, Lippold JC, Brandi SD (2003) The relationship between chromium nitride and secondary austenite precipitation in duplex stainless steels. Metall Mater Trans A 34(8):1575–1597. https://doi.org/10.1007/s11661-003-0304-9
53. Muthupandi V, Bala Srinivasan P, Seshadri SK, Sundaresan S (2003) Effect of weld metal chemistry and heat input on the structure and properties of duplex stainless steel welds. Mater Sci Eng A 358(1–2):9–16. https://doi.org/10.1016/S0921-5093(03)00077-7
54. Saravanan S, Sivagurumanikandan N, Raghukandan K (2019) Effect of heat input on microstructure and mechanical properties of Nd:YAG laser welded super duplex stainless steel – numerical and experimental approach. Optik 185:447–455. https://doi.org/10.1016/j.ijleo.2019.03.145
55. Kolenic F, Kovac L, Drimal D (2011) Effect of laser welding conditions on austenite/ferrite ratio in duplex stainless steel 2507 welds. Weld World 55(5–6):19–25. https://doi.org/10.1007/BF03321292
56. da Cruz Junior EJ, Franzini OD, Calliari I, Ventrella VA (2019) Effects of nickel addition on the microstructure of laser-welded UNS S32750 duplex stainless steel. Metall Mater Trans A 50(4):1616–1618. https://doi.org/10.1007/s11661-019-05115-1
57. Zhang Z, Jing H, Xu L, Han Y, Zhao L (2017) Influence of microstructure and elemental partitioning on pitting corrosion resistance of duplex stainless steel welding joints. Appl Surf Sci 394:297–314. https://doi.org/10.1016/j.apsusc.2016.10.047
58. Ha HY, Jang MH, Lee TH, Moon J (2015) Understanding the relation between phase fraction and pitting corrosion resistance of UNS S32750 stainless steel. Mater Charact 106:338–345. https://doi.org/10.1016/j.matchar.2015.06.019
59. Hertzman S, Huhtala T, Karlsson L, Nilsson JO, Nilsson M, Jargelius-Pettersson R, Wilson A (1997) Microstructure–property relations of Mo- and W-alloyed super duplex stainless weld metals. Mater Sci Technol 13(7):604–613. https://doi.org/10.1179/mst.1997.13.7.604
60. Hosseini VA, Wessman S, Hurtig K, Karlsson L (2016) Nitrogen loss and effects on microstructure in multipass TIG welding of a super duplex stainless steel. Mater Des 98:88–97. https://doi.org/10.1016/j.matdes.2016.03.011
61. Hosseini VA, Karlsson L (2019) Physical and kinetic simulation of nitrogen loss in high temperature heat affected zone of duplex stainless steels. Materialia 6:100325. https://doi.org/10.1016/j.mtla.2019.100325

62. Varbai B, Májlinger K (2019) Physical and theoretical modeling of the nitrogen content of duplex stainless steel weld metal: shielding gas composition and heat input effects. Metals 9(7):762. https://doi.org/10.3390/met9070762
63. Pardal JM, Tavares SSM, Fonseca MC, de Souza JA, Côrte RRA, de Abreu HFG (2009) Influence of the grain size on deleterious phase precipitation in superduplex stainless steel UNS S32750. Mater Charact 60(3):165–172. https://doi.org/10.1016/j.matchar.2008.08.007
64. Escriba DM, Materna-Morris E, Plaut RL, Padilha AF (2009) Chi-phase precipitation in a duplex stainless steel. Mater Charact 60(11):1214–1219. https://doi.org/10.1016/j.matchar.2009.04.013
65. Holländer Pettersson N, Lindell D, Lindberg F, Borgenstam A (2019) Formation of chromium nitride and intragranular austenite in a super duplex stainless steel. Metall Mater Trans A 50(12):5594–5601. https://doi.org/10.1007/s11661-019-05489-2
66. Nilsson JO, Karlsson L, Andersson JO (1995) Secondary austenite formation and its relation to pitting corrosion in duplex stainless steel weld metal. Mater Sci Technol 11(3):276–283. https://doi.org/10.1179/mst.1995.11.3.276
67. Wu XH, Song ZG, Wang BS, Wu MH, Nai QL, Yao L, Feng H, Zheng WJ (2022) Morphologies of secondary austenite in 2507 duplex stainless steel after heat treatment. J Iron Steel Res Int 29(6):994–1003. https://doi.org/10.1007/s42243-021-00660-9
68. Vacchi GS, Magalhães DCC, Mendes Filho AA, Cintho OM, Meinhardt CP, Bergmann LA, Rovere CAD (2025) Microstructural evolution and localized corrosion behavior of friction stir welded super duplex UNS S32760 in chloride-containing environments. J Mater Res Technol 36:481–499. https://doi.org/10.1016/j.jmrt.2025.03.042
69. Tavares SSM, Pardal JM, Lima LD, Bastos IN, Nascimento AM, de Souza JA (2007) Characterization of microstructure, chemical composition, corrosion resistance and toughness of a multipass weld joint of superduplex stainless steel UNS S32750. Mater Charact 58(7):610–616. https://doi.org/10.1016/j.matchar.2006.07.006
70. Prasad R, Yuvaraj N, Vipin (2026) Microstructure and mechanical characterization of dissimilar super duplex stainless steel 2507–Inconel 718 alloy structure built by cold metal transfer-based wire arc directed energy deposition. J Mater Eng Perform 35(4):3264–3274. https://doi.org/10.1007/s11665-025-11823-0
71. Kumar P, Maji K (2024) Experimental investigations and parametric effects on depositions of super duplex stainless steel in wire arc additive manufacturing. Proc Inst

Mech Eng E J Process Mech Eng 238(4):1600–1612. https://doi.org/10.1177/09544089231158253
72. Hu Y, Xue J (2023) Effects of flowrate of additional shielding gas on the properties of welded seam using twin-wire GMAW welding for duplex stainless steel. Metals 13(7):1224. https://doi.org/10.3390/met13071224
73. Weis S, Grunert R, Brumm S, Halmaghi M, Prank U (2024) Comparative study between TIG-MIG hybrid and MIG welding of 1.4462 duplex steel joints. Weld World 68(1):51–59. https://doi.org/10.1007/s40194-023-01620-5
74. Qi K, Li RF, Wang GJ, Sun Z (2019) Structure and mechanical properties of laser-MIG hybrid welded SAF 2507 super duplex stainless steel joints. Int J Mod Phys B 33(01n03):1940037. https://doi.org/10.1142/S021797921940037X
75. Acherjee B (2018) Hybrid laser arc welding: state-of-art review. Opt Laser Technol 99:60–71. https://doi.org/10.1016/j.optlastec.2017.09.038
76. Zhang Z, Jing H, Xu L, Han Y, Zhao L (2017) The influence of microstructural evolution on selective corrosion in duplex stainless steel flux-cored arc welded joints. Corros Sci 120:194–210. https://doi.org/10.1016/j.corsci.2016.12.007
77. Taban E (2008) Toughness and microstructural analysis of superduplex stainless steel joined by plasma arc welding. J Mater Sci 43(12):4309–4315. https://doi.org/10.1007/s10853-008-2632-z
78. Wang Q, Gu G, Jia C, Li K, Wu C (2023) Investigation of microstructure evolution, mechanical and corrosion properties of SAF 2507 super duplex stainless steel joints by keyhole plasma arc welding. J Mater Res Technol 22:355–374. https://doi.org/10.1016/j.jmrt.2022.11.107
79. Ramkumar KD, Mishra D, Vignesh MK, Ganesh Raj B, Arivazhagan N, Naren SV, Suresh Kumar S (2014) Metallurgical and mechanical characterization of electron beam welded super-duplex stainless steel UNS 32750. J Manuf Process 16(4):527–534. https://doi.org/10.1016/j.jmapro.2014.07.011
80. Šimeková B, Dománková M, Kovaříková I, Kovačócy P, Martinkovič M, Šimek M, Ciuła L (2024) Microstructural and mechanical characterization of the laser beam welded SAF 2507 super-duplex stainless steel. Metals 14(10):1184. https://doi.org/10.3390/met14101184
81. Sato YS, Nelson TW, Sterling CJ, Steel RJ, Pettersson CO (2005) Microstructure and mechanical properties of friction stir welded SAF 2507 super duplex stainless steel. Mater Sci Eng A 397(1–2):376–384. https://doi.org/10.1016/j.msea.2005.02.054

82. Brum Walter NM, Braga Lemos GV, Kieckow GS, Buzzatti DT, Buzzatti JT, Mattei F et al (2024) Investigating microstructure, mechanical properties, and pitting corrosion resistance of UNS S32760 super duplex stainless steel after linear friction welding. J Mater Res Technol 31:1637–1643. https://doi.org/10.1016/j.jmrt.2024.06.191
83. Tathgir S, Rathod DW, Batish A (2019) A-TIG welding process for enhanced-penetration in duplex stainless-steel: effect of activated fluxes. Mater Manuf Process 34(14):1659–1670. https://doi.org/10.1080/10426914.2019.1666990
84. Giorjão RAR, Pereira VF, Terada M, da Fonseca EB, Marinho RR, Garcia DM, Tschiptschin AP (2019) Microstructure and mechanical properties of friction stir welded 8 mm pipe SAF 2507 super duplex stainless steel. J Mater Res Technol 8(1):243–249. https://doi.org/10.1016/j.jmrt.2018.01.002
85. Maurya AK, Chhibber R, Pandey C (2023) Heat input effect on dissimilar super duplex stainless steel (UNS S32750) and Nitronic steel (N 50) gas tungsten arc weld: mechanism, microstructure, and mechanical properties. J Mater Eng Perform 32(12):5283–5316. https://doi.org/10.1007/s11665-022-07471-3
86. Hosseini VA, Valiente Bermejo MA, Gårdstam J, Hurtig K, Karlsson L (2016) Influence of multiple thermal cycles on microstructure of heat-affected zone in TIG-welded super duplex stainless steel. Weld World 60(2):233–245. https://doi.org/10.1007/s40194-016-0300-5
87. Valiente Bermejo MA, Hurtig K, Eyzop D, Karlsson L (2019) A new approach to the study of multi-pass welds – microstructure and properties of welded 20-mm-thick superduplex stainless steel. Appl Sci 9(6):1050. https://doi.org/10.3390/app9061050
88. Chacón-Fernández S, Portolés-García A, Romaní-Labanda G (2022) Analysis of the influence of GMAW process parameters on the properties and microstructure of S32001 steel. Materials 15(18):6498. https://doi.org/10.3390/ma15186498
89. Paulraj P, Garg R (2016) Effect of welding parameters on pitting behavior of GTAW of DSS and super DSS weldments. Eng Sci Technol Int J 19(2):1076–1083. https://doi.org/10.1016/j.jestch.2016.01.013
90. Kumar R, Agrawal AP, Maurya M, Ali S, Giri MK, Kumar A, Maurya NK (2026) Influence of heat input on phase balance, microstructural evolution, and mechanical performance of super duplex stainless steel welded by gas tungsten arc welding. J Mater Eng Perform 35(29):30399–30406. https://doi.org/10.1007/s11665-026-13845-8

91. Westin EM, Wessman S (2024) Characteristics of high-temperature heat-affected zones in duplex stainless steels. Weld World 68(8):1981–1997. https://doi.org/10.1007/s40194-024-01715-7
92. Landowski M, Simon SC, Breznay C, Fydrych D, Varbai B (2024) Effects of preheating on laser beam–welded NSSC 2120 lean duplex steel. Int J Adv Manuf Technol 130:2009–2021. https://doi.org/10.1007/s00170-023-12840-w
93. Prunbauer M, Raninger P, Ecker W, Rester M, Ebner R (2024) A comprehensive material model for the super-duplex stainless steel SAF2507 in a welding environment. Metals 14(2):153. https://doi.org/10.3390/met14020153
94. Sathiya P, Aravindan S, Soundararajan R, Noorul Haq A (2009) Effect of shielding gases on mechanical and metallurgical properties of duplex stainless-steel welds. J Mater Sci 44(1):114–121. https://doi.org/10.1007/s10853-008-3098-8
95. Huang X, Qiu W, Niu B, Zou X, Pan L, Kwok CT (2024) Role of complex nonmetallic inclusions on the localized corrosion resistance of wire arc additively manufactured super duplex stainless steel. J Mater Res Technol 28:799–813. https://doi.org/10.1016/j.jmrt.2023.12.072
96. Iams AD, Keist JS, Giannuzzi LA, Palmer TA (2021) The evolution of oxygen-based inclusions in an additively manufactured super-duplex stainless steel. Metall Mater Trans A 52(8):3401–3412. https://doi.org/10.1007/s11661-021-06311-8
97. Zhang Z, Jing H, Xu L, Han Y, Zhao L, Zhou C (2017) Effects of nitrogen in shielding gas on microstructure evolution and localized corrosion behavior of duplex stainless steel welding joint. Appl Surf Sci 404:110–128. https://doi.org/10.1016/j.apsusc.2017.01.252
98. Rodriguez-Vargas BR, Stornelli G, Miranda Pérez AF, Di Schino A (2024) Effect of nitrogen-added shielding gas on microstructure evolution of welded joints by gas tungsten arc welding process in duplex stainless steel 2205. Steel Res Int 95(5):2300798. https://doi.org/10.1002/srin.202300798
99. Kim ST, Jang SH, Lee IS, Park YS (2011) Effects of solution heat-treatment and nitrogen in shielding gas on the resistance to pitting corrosion of hyper duplex stainless steel welds. Corros Sci 53(5):1939–1947. https://doi.org/10.1016/j.corsci.2011.02.013
100. Migiakis K, Papadimitriou GD (2009) Effect of nitrogen and nickel on the microstructure and mechanical properties of plasma welded UNS S32760 super-duplex stainless steels. J Mater Sci 44(23):6372–6383. https://doi.org/10.1007/s10853-009-3878-9

101. Pilhagen J, Sandström R (2014) Influence of nickel on the toughness of lean duplex stainless steel welds. Mater Sci Eng A 602:49–57. https://doi.org/10.1016/j.msea.2014.01.093
102. Kangazian J, Shamanian M (2019) Effect of pulsed current on the microstructure, mechanical properties and corrosion behavior of Ni-based alloy/super duplex stainless steel dissimilar welds. Trans Indian Inst Met 72(9):2403–2416. https://doi.org/10.1007/s12666-019-01693-1
103. Maurya AK, Pandey SM, Chhibber R, Fydrych D, Pandey C (2024) Corrosion performance of super duplex stainless steel and pipeline steel dissimilar welded joints: a comprehensive investigation for marine structures. Int J Adv Manuf Technol 135:1009–1033. https://doi.org/10.1007/s00170-024-14596-3
104. Higelin A, Le Manchet S, Passot G, Cissé S, Grocki J (2022) Heat-affected zone ferrite content control of a duplex stainless steel grade to enhance weldability. Weld World 66(8):1503–1519. https://doi.org/10.1007/s40194-022-01326-0
105. Devendranath Ramkumar K, Thiruvengatam G, Sudharsan SP, Mishra D, Arivazhagan N, Sridhar R (2014) Characterization of weld strength and impact toughness in the multi-pass welding of super-duplex stainless steel UNS 32750. Mater Des 60:125–135. https://doi.org/10.1016/j.matdes.2014.03.031
106. Zhang Z, Zhang H, Hu J, Qi X, Bian Y, Shen A, Xu P, Zhao Y (2018) Microstructure evolution and mechanical properties of briefly heat-treated SAF 2507 super duplex stainless steel welds. Constr Build Mater 168:338–345. https://doi.org/10.1016/j.conbuildmat.2018.02.143
107. Standards Norway (2004) NORSOK Standard M-601: welding and inspection of piping. Standards Norway, Lysaker
108. Vahman M, Shamanian M, Golozar MA, Jalali A, Sarmadi MA, Kangazian J (2020) The effect of welding heat input on the structure–property relationship of a new grade super duplex stainless steel. Steel Res Int 91:1900347. https://doi.org/10.1002/srin.201900347
109. Vucko F, Ringot G, Thierry D, Larché N (2022) Fatigue behavior of super duplex stainless steel exposed in natural seawater under cathodic protection. Front Mater 9:826189. https://doi.org/10.3389/fmats.2022.826189
110. Ma CY, Zhou L, Zhang RX, Li DG, Shu FY, Song XG, Zhao YQ (2020) Enhancement in mechanical properties and corrosion resistance of 2507 duplex stainless steel via friction stir processing. J Mater Res Technol 9(4):8296–8305. https://doi.org/10.1016/j.jmrt.2020.05.057

111. Perren RA, Suter TA, Uggowitzer PJ, Weber L, Magdowski R, Böhni H, Speidel MO (2001) Corrosion resistance of super duplex stainless steels in chloride ion containing environments: investigations by means of a new microelectrochemical method. I. Precipitation-free states. Corros Sci 43(4):707–726. https://doi.org/10.1016/S0010-938X(00)00087-1
112. Perren RA, Suter T, Solenthaler C, Gullo G, Uggowitzer PJ, Böhni H, Speidel MO (2001) Corrosion resistance of super duplex stainless steels in chloride ion containing environments: investigations by means of a new microelectrochemical method. II. Influence of precipitates. Corros Sci 43(4):727–745. https://doi.org/10.1016/S0010-938X(00)00088-3
113. Ha HY, Jang MH, Lee TH, Moon J (2014) Interpretation of the relation between ferrite fraction and pitting corrosion resistance of commercial 2205 duplex stainless steel. Corros Sci 89:154–162. https://doi.org/10.1016/j.corsci.2014.08.021
114. Kang DH, Lee HW (2013) Study of the correlation between pitting corrosion and the component ratio of the dual phase in duplex stainless steel welds. Corros Sci 74:396–407. https://doi.org/10.1016/j.corsci.2013.04.033
115. Hou Y, Nakamori Y, Kadoi K, Inoue H, Baba H (2022) Initiation mechanism of pitting corrosion in weld heat affected zone of duplex stainless steel. Corros Sci 201:110278. https://doi.org/10.1016/j.corsci.2022.110278
116. Shen K, Jiang W, Sun C, Zhao W, Sun J (2022) Unlocking the influence of microstructural evolution on hardness and pitting corrosion in duplex stainless welded joints. Corros Sci 206:110532. https://doi.org/10.1016/j.corsci.2022.110532
117. Cui Z, Chen S, Dou Y, Han S, Wang L, Man C, Wang X, Chen S, Cheng YF, Li X (2019) Passivation behavior and surface chemistry of 2507 super duplex stainless steel in artificial seawater: influence of dissolved oxygen and pH. Corros Sci 150:218–234. https://doi.org/10.1016/j.corsci.2019.02.002
118. Rahimi E, Kosari A, Hosseinpour S, Davoodi A, Zandbergen H, Mol JMC (2019) Characterization of the passive layer on ferrite and austenite phases of super duplex stainless steel. Appl Surf Sci 496:143634. https://doi.org/10.1016/j.apsusc.2019.143634
119. Cui ZY, Wang LW, Ni HT, Hao WK, Man C, Chen SS, Wang X, Liu ZY, Li XG (2017) Influence of temperature on the electrochemical and passivation behavior of 2507 super duplex stainless steel in simulated desulfurized flue gas condensates. Corros Sci 118:31–48. https://doi.org/10.1016/j.corsci.2017.01.016

120. Hong J, Han D, Tan H, Li J, Jiang Y (2013) Evaluation of aged duplex stainless steel UNS S32750 susceptibility to intergranular corrosion by optimized double loop electrochemical potentiokinetic reactivation method. Corros Sci 68:249–255. https://doi.org/10.1016/j.corsci.2012.11.024
121. Song L, Liu Z, Li X, Du C (2020) Stress corrosion cracking of 2205 duplex stainless steel with simulated welding microstructures in simulated sea environment at different depths. J Mater Eng Perform 29(8):5476–5489. https://doi.org/10.1007/s11665-020-05052-w
122. Meinhardt CP, Scheid A, dos Santos JF, Bergmann LA, Favaro MB, Fortis Kwietniewski CE (2017) Hydrogen embrittlement under cathodic protection of friction stir welded UNS S32760 super duplex stainless steel. Mater Sci Eng A 706:48–56. https://doi.org/10.1016/j.msea.2017.08.117
123. Cervo R, Ferro P, Tiziani A (2010) Annealing temperature effects on super duplex stainless steel UNS S32750 welded joints. I: microstructure and partitioning of elements. J Mater Sci 45(16):4369–4377. https://doi.org/10.1007/s10853-010-4310-1
124. Saravanan S, Raghukandan K, Sivagurumanikandan N (2017) Pulsed Nd:YAG laser welding and subsequent post-weld heat treatment on super duplex stainless steel. J Manuf Process 25:284–289. https://doi.org/10.1016/j.jmapro.2016.12.015
125. Pinheiro FW, de Souza LM, Pereira EC, Monteiro SN, Azevedo ARG (2023) Effect of solubilization heat treatment on microstructure and corrosion resistance of joints welded with the autogenous TIG process duplex stainless steel. J Mater Res Technol 26:1527–1536. https://doi.org/10.1016/j.jmrt.2023.08.014
126. Li J, Shen W, Lin P, Wang F, Yang Z (2020) Effect of solution treatment temperature on microstructural evolution, precipitation behavior, and comprehensive properties in UNS S32750 super duplex stainless steel. Metals 10(11):1481. https://doi.org/10.3390/met10111481
127. Shen W, Wang F, Yang Z, Sun L, Li Y, Jin J (2021) Effect of ferrite proportion and precipitates on dual-phase corrosion of S32750 super duplex stainless steel with different annealing temperatures. Steel Res Int 92(6):2000568. https://doi.org/10.1002/srin.202000568
128. Ferrari E, Colombini E, Giovanardi R, Zaniboni F, Gaiani S, Veronesi P (2025) Effect of shielding gas and post-welding heat treatment on the mechanical and corrosion performances of duplex and super duplex stainless steels' low heat-input welded joints. Materials 18(21):4818. https://doi.org/10.3390/ma18214818

129. da Cruz Junior EJ, Seloto BB, Ventrella VA, Varasquim FMFA, Zambon A, Calliari I, Gennari C, Settimi AG (2023) Correction of phase balance on Nd:YAG pulsed laser welded UNS S32750 using cobalt electroplating technique. Crystals 13(2):256. https://doi.org/10.3390/cryst13020256
130. Akselsen OM, Bjørge R, Ånes HW, Ren X, Nyhus B (2021) Effect of sigma phase in wire arc additive manufacturing of superduplex stainless steel. Metals 11(12):2045. https://doi.org/10.3390/met11122045
131. Akbarzadeh E, Yurtışık K, Gür CH, Saeid T, Tavangar R (2024) Influence of shielding gas on the microstructure and mechanical properties of duplex stainless steel in wire arc additive manufacturing. Met Mater Int 30(7):1977–1996. https://doi.org/10.1007/s12540-023-01623-3
132. Kou S (2003) Welding metallurgy. 2nd ed. John Wiley & Sons, Hoboken, NJ
133. Qi K, Li RF, Wang GJ, Li GZ, Liu B, Wu MF (2019) Microstructure and corrosion properties of laser-welded SAF 2507 super duplex stainless steel joints. J Mater Eng Perform 28(1):287–295. https://doi.org/10.1007/s11665-018-3833-5
134. Beziou O, Hamdi I, Boumerzoug Z, Brisset F, Baudin T (2023) Effect of heat treatment on the welded joint of X70 steel joined to duplex stainless steel by gas tungsten arc welding. Int J Adv Manuf Technol 127:2799–2814. https://doi.org/10.1007/s00170-023-11675-9
135. Kangazian J, Shamanian M, Kim HS (2025) Microstructural evolution, strength-ductility synergy, and corrosion behavior of the UNS N08825 Ni-based superalloy/UNS S32750 super duplex stainless steel friction stir welds. J Mater Res Technol 37:583–600. https://doi.org/10.1016/j.jmrt.2025.06.064
136. ASTM International (2008) ASTM A923-08: standard test methods for detecting detrimental intermetallic phase in duplex austenitic/ferritic stainless steels. ASTM International, West Conshohocken, PA
137. Lopes BLS, Rodrigues SF, Silva ES, Reis GS, Martins WDP, Damascena JC et al (2018) Influence of MIG/MAG welding process on mechanical and pitting corrosion behaviors on the super-duplex stainless steel SAF 2507 welded joints. Mater Sci Appl 9(2):228–245. https://doi.org/10.4236/msa.2018.92015
138. Rasmussen CE, Williams CKI (2006) Gaussian processes for machine learning. MIT Press, Cambridge, MA. https://doi.org/10.7551/mitpress/3206.001.0001

139. Schulz E, Speekenbrink M, Krause A (2018) A tutorial on Gaussian process regression: modelling, exploring, and exploiting functions. J Math Psychol 85:1–16. https://doi.org/10.1016/j.jmp.2018.03.001
140. Deringer VL, Bartók AP, Bernstein N, Wilkins DM, Ceriotti M, Csányi G (2021) Gaussian process regression for materials and molecules. Chem Rev 121(16):10073–10141. https://doi.org/10.1021/acs.chemrev.1c00022
141. Sterling D, Sterling T, Zhang Y, Chen H (2015) Welding parameter optimization based on Gaussian process regression Bayesian optimization algorithm. In: 2015 IEEE International Conference on Automation Science and Engineering (CASE); Gothenburg, Sweden:1490–1496. https://doi.org/10.1109/CoASE.2015.7294310
142. Dong H, Cong M, Liu Y, Zhang Y, Chen H (2016) Predicting characteristic performance for arc welding process. In: 2016 IEEE International Conference on Cyber Technology in Automation, Control and Intelligent Systems (CYBER); Chengdu, China:7–12. https://doi.org/10.1109/CYBER.2016.7574786
143. Kim JY, Lee DY, Lee J, Lee SH (2021) Parameter optimization of hybrid-tandem gas metal arc welding using analysis of variance-based Gaussian process regression. Metals 11(7):1087. https://doi.org/10.3390/met11071087
144. Lee SH (2020) Optimization of cold metal transfer-based wire arc additive manufacturing processes using Gaussian process regression. Metals 10(4):461. https://doi.org/10.3390/met10040461
145. Verma S, Gupta M, Misra JP (2018) Performance evaluation of friction stir welding using machine learning approaches. MethodsX 5:1048–1058. https://doi.org/10.1016/j.mex.2018.09.002
146. Hartl R, Vieltorf F, Benker M, Zaeh MF (2020) Predicting the ultimate tensile strength of friction stir welds using Gaussian process regression. J Manuf Mater Process 4(3):75. https://doi.org/10.3390/jmmp4030075
147. Haas M, Onuseit V, Powell J, Zaiss F, Wahl J, Menold T, Hagenlocher C, Michalowski A (2024) Improving the weld seam quality in laser welding processes by means of Bayesian optimization. Procedia CIRP 124:772–775. https://doi.org/10.1016/j.procir.2024.08.222
148. Haas M, Steinhoff R, Powell J, Zaiß F, Wahl J, Hagenlocher C et al (2026) Efficient parameter selection in laser welding via Bayesian optimization. J Intell Manuf:1–17. https://doi.org/10.1007/s10845-026-02799-2

149. Menold T, Onuseit V, Buser M, Haas M, Bär N, Michalowski A (2024) Laser material processing optimization using Bayesian optimization: a generic tool. Light Adv Manuf 5(3):355–365. https://doi.org/10.37188/lam.2024.032
150. Chepiga T, Zhilyaev P, Ryabov A, Simonov AP, Dubinin ON, Firsov DG, Kuzminova YO, Evlashin SA (2023) Process parameter selection for production of stainless steel 316L using efficient multi-objective Bayesian optimization algorithm. Materials 16(3):1050. https://doi.org/10.3390/ma16031050
151. Tapia G, Elwany AH, Sang H (2016) Prediction of porosity in metal-based additive manufacturing using spatial Gaussian process models. Addit Manuf 12:282–290. https://doi.org/10.1016/j.addma.2016.05.009
152. Itano K, Takahashi H, Fukumoto M (2026) Predicting the corrosion resistance of Fe–Cr alloys in ammonia environments using Gaussian process regression. High Temp Corros Mater 103:47. https://doi.org/10.1007/s11085-026-10403-4
153. Kumar P, Mondal S, Maji K (2025) Analysis and optimization of super duplex stainless steel deposition in wire arc additive manufacturing using machine learning techniques. SAE Int J Mater Manuf 18(1):109–122. https://doi.org/10.4271/05-18-01-0008
154. Hou F, Wu HH, Zhu D, Zhang J, Hou L, Wang S et al (2025) Interpretable material descriptors for critical pitting temperature in austenitic stainless steel via machine learning. NPJ Mater Degrad 9:16. https://doi.org/10.1038/s41529-025-00563-0
155. Duvenaud D (2014) Automatic model construction with Gaussian processes. Dissertation, University of Cambridge. https://doi.org/10.17863/CAM.14087
156. Sacks J, Welch WJ, Mitchell TJ, Wynn HP (1989) Design and analysis of computer experiments. Stat Sci 4(4):409–423. https://doi.org/10.1214/ss/1177012413
157. Kennedy MC, O'Hagan A (2001) Bayesian calibration of computer models. J R Stat Soc Series B Stat Methodol 63(3):425–464. https://doi.org/10.1111/1467-9868.00294
158. Jones DR, Schonlau M, Welch WJ (1998) Efficient global optimization of expensive black-box functions. J Glob Optim 13(4):455–492. https://doi.org/10.1023/A:1008306431147
159. Srinivas N, Krause A, Kakade SM, Seeger MW (2012) Information-theoretic regret bounds for Gaussian process optimization in the bandit setting. IEEE Trans Inf Theory 58(5):3250–3265. https://doi.org/10.1109/TIT.2011.2182033
160. Shahriari B, Swersky K, Wang Z, Adams RP, de Freitas N (2016) Taking the human out of the loop: a review of Bayesian optimization. Proc IEEE 104(1):148–175. https://doi.org/10.1109/JPROC.2015.2494218

161. Garnett R (2023) Bayesian optimization. Cambridge University Press, Cambridge. https://doi.org/10.1017/9781108348973
162. Wang X, Jin Y, Schmitt S, Olhofer M (2023) Recent advances in Bayesian optimization. ACM Comput Surv 55(13s):287. https://doi.org/10.1145/3582078

Appendix A. Search strings and abbreviations

A.1 Search strings

• ("super duplex" OR "UNS S32750" OR "SAF 2507" OR "2507" OR "25Cr duplex") AND ("gas metal arc" OR GMAW OR MIG OR MAG OR "pulsed GMAW")

• ("super duplex" OR "UNS S32750" OR "ER2594") AND ("cold metal transfer" OR CMT OR "wire arc additive" OR WAAM)

• ("duplex stainless" OR "super duplex") AND weld* AND ("heat input" OR "arc energy" OR "interpass" OR "multipass" OR "reheating")

• ("duplex stainless" OR "super duplex") AND weld* AND ("shielding gas" OR "backing gas" OR nitrogen OR "Ar-N2" OR "Ar-He")

• ("super duplex" OR "UNS S32750") AND ("sigma phase" OR "chromium nitride" OR "secondary austenite" OR "chi phase")

• ("super duplex" OR "UNS S32750") AND weld* AND ("pitting" OR "critical pitting temperature" OR "toughness" OR "hydrogen")

• ("Gaussian process regression" OR "Gaussian process" OR kriging OR "Bayesian optimization") AND (weld* OR "wire arc additive" OR "additive manufacturing" OR corrosion OR pitting)

Searches were limited to English-language journal articles, standards and guidelines; publication years 2018–2026 were prioritised, with earlier sources retained where they remain the primary evidence for a mechanism.

A.2 Thermal-efficiency basis of compiled heat-input data

The efficiency used by each author, the EN 1011-1 factor applied in this review and the resulting net heat input for every compiled heat-input data set are listed in Table A1.

Table A1 Thermal-efficiency basis of the heat-input data compiled in this review and conversion to net heat input with the EN 1011-1 thermal efficiency factors (k)

Ref.	Process	Quantity reported by authors	Efficiency used by authors	Reported values (kJ mm^{-1})	Arc energy (kJ mm^{-1})	k (EN 1011-1)	Net heat input (kJ mm^{-1})
[6]	Pulsed GMAW	Arc energy	1.0	1.18–1.58	1.18–1.58	0.8	0.94–1.26
[6]	SAW	Arc energy	1.0	1.2–1.5; 2.0–2.3	1.2–1.5; 2.0–2.3	1.0	1.2–1.5; 2.0–2.3
[16]	GTAW	Heat input, $\eta = 1$	1.0	0.78, 0.99, 1.22, 1.47	0.78, 0.99, 1.22, 1.47	0.6	0.47, 0.59, 0.73, 0.88
[36]	GTAW	Welding energy	Not stated	0.5, 1.0, 3.5	0.5, 1.0, 3.5 (assumed)	0.6	0.30, 0.60, 2.10
[35]	SMAW	Heat input	0.65	0.80 (ER2594); 0.74 (ER2595)	1.23; 1.14	0.8	0.99; 0.92
[18]	Robotic GMAW	Heat input	0.8	0.62, 0.52, 0.44	0.77, 0.65, 0.55	0.8	0.62, 0.52, 0.44
[4]	Guideline (all arc processes)	Heat input = U·I/v	1.0 (none applied)	0.3–1.5 (2507)	0.3–1.5	–	Process-dependent; window kept in arc energy (Fig. 12)

Arc energy $E = U \cdot I/v$; net heat input $Q = k \cdot E$ [37]. Values reported with an author-specific efficiency were first divided by that efficiency to recover the arc energy. Where no efficiency was stated, the reported value was treated as arc energy; this assumption is flagged. All heat-input axes in Figs. 7 and 8 are net heat input.

A.3 Abbreviations

BM: base metal

CMT: cold metal transfer

CPT: critical pitting temperature

CVN: Charpy V-notch

DL-EPR: double-loop electrochemical potentiokinetic reactivation

DOS: degree of sensitisation

DSS: duplex stainless steel

EAC: environmentally assisted cracking

EBW: electron beam welding

FCAW: flux-cored arc welding

FSW: friction stir welding

FZ: fusion zone

GBA: grain-boundary austenite

GMAW: gas metal arc welding

GTAW: gas tungsten arc welding

HAZ: heat-affected zone (HT-, high-temperature; LT-, low-temperature)

HI: heat input

HISC: hydrogen-induced stress cracking

IGA: intragranular austenite

IP: interpass temperature

LBW: laser beam welding

LFW: linear friction welding

PREN: pitting resistance equivalent number

PWHT: post-weld heat treatment

SAW: submerged arc welding

SCC: stress corrosion cracking

SDSS: super duplex stainless steel

SMAW: shielded metal arc welding

WA: Widmanstätten austenite

WAAM: wire-arc additive manufacturing

WM: weld metal

γ_2: secondary austenite

$\Delta t_{12/8}$: cooling time from 1200 to 800 °C